Sr-Nd isotopic characteristics of the Kanmantoo Cu-Au deposit

Thesis submitted in accordance with the requirements of the University of Adelaide for an Honours Degree in Geology/Geophysics

William James Rowe

November 2020

SR-ND ISOTOPIC CHARACTERISTICS OF THE KANMANTOO CU-AU DEPOSIT

KANMANTOO CU-AU DEPOSIT GEOCHEMISTRY

ABSTRACT

The Kanmantoo Cu-Au mine located 50km south-east of Adelaide hosts Delamerian mineralization debated to be epigenetic metamorphogenic with a degree of magmatic input or a syn-sedimentary origin. Studying existing mines within the Delamerian in combination with the sources of fluids and metals the deposit is derived from is fundamental in characterising the exploration potential in South Australia. This study consists of documenting 8 Kanmantoo mine samples and allocating the samples into groups based on hydrothermal, granitic and host rock origin. Hand samples, thin sections, geochemistry, and Sr-Nd isotopes have been analysed to constrain characteristics of the mine that determine geological formation. Sr-Nd isotope analysis was conducted at the University of Adelaide clean laboratories and involved acid digestion, column chemistry and thermal ionization mass spectrometry. The study distinguishes εNd values age corrected for 500Ma that indicate the most juvenile samples studied in the Kanmantoo to be the Fule aluminous vein (εNd -11.4) and BK25 sulphide vein (εNd -12.3), Proximal host rocks (εNd -14.9) and distal host rocks (εNd -14.3) recorded less juvenile signatures compared to Kanmantoo samples studied. The samples studied in this thesis indicate isotopic correlation most closely associated with Delamerian S-type granites, providing evidence mineralization was not derived from an I-type source and formed from the partial melting of supracrustal rocks. The absence of an isotopic signature recognizing a nearby mantle-derived source indicates the ore-bearing fluid was deposited from a synmetamorphic hydrothermal system.

KEYWORDS

Kanmantoo, Delamerian orogeny, hydrothermal mineralisation, geochemistry, Sr-Nd isotopes, exploration

Word Count 7919

Contents

LIST OF FIGURES AND TABLES

1. INTRODUCTION

The Kanmantoo Cu-Au located 52km South East of Adelaide hosts Delamerian mineralization that is often speculated to have some form of syn- to post-peak metamorphic hydrothermal input (Kimpton 2018; Morgan 2019; Foden et al., 1999). The Kanmantoo Cu-Au mine's formation has previously been cited to be caused by a hydrothermal or magmatic genesis (Kimpton 2018; Morgan 2019; Oliver et al., 1998) and this thesis aims to understand the formation of the ore deposit through the collection of data on the sources of fluids and metals composing the mineralization, granitic intrusions and regional host rocks within a close proximity to the Kanmantoo tenement. Characterising the genesis of the mineralization in the Kanmantoo deposit has the potential to be extrapolated to the greater Delamerian expanse with hopes of future exploration occurring in South-Eastern South Australia, amidst a future characterised by increasing exploration investment and decreasing average global ore grade (Calvo et.al 2016; Rötzer & Schmidt 2018). Kanmantoo fluid sources are heavily debated with theories of a magmatic source, hydrothermal metamorphism, and sedimentary exhalative genesis responsible for the mineralization. Hydrothermal ore-forming processes are present universally and it is scarce to find ore deposits on Earth that have not been formed by a hot aqueous solution, of which Kanmantoo is no exception (Oliver et al., 1998). Determining the degree a hydrothermal fluid has been flown through or replaced the host is essential in determining the mineralization of a deposit (Robb, 2005). Fluid mixing of hydrothermal and magmatic sources promotes the precipitation of metals from ore-forming fluids (Yardley & Cleverley, 2015) (Robb, 2005) and states to further contributes to the controversy regarding the genesis at the Kanmantoo Cu-au

deposit, as it is classified as a complex ore deposit where a combination of different processes and models have been proposed.

Potential sources of metals at the Kanmantoo have been theorized to be directly sourced from mantle-derived magmas, or through the scavenging of pre-existing surficial features (Pollock et al., 2018; Seccombe et al., 1985; Tomkins, 2013; Richards, 2013). The sourcing of fluid and metals is shrouded in controversy regarding the derivation of source material from surrounding rocks, or if the derivation was the product of a magmatic mantle source contribution (Pollock et al., 2018; Seccombe et al., 1985). A unique combination of events is required to transpire to form an orebody, and it necessitates several techniques to unravel the various source contributions (Richards, 2013). Literature proposing models for igneous, sedimentary, or metamorphic mineral genesis is significant to the exploration of other deposits in the Delamerian orogeny as it emphasizes the necessity to look for a syngenetic or epigenetic deposit (Robb, 2005) (Lovering 1963). This investigation aims to examine hand samples, thin sections, geochemistry, Sr-Nd isotopes and Delamerian literature to constrain the characteristics of the mine and investigate the potential role of mantle contribution to fluids or metals of syn-metamorphic formation in the Kanmantoo deposit (Oliver et al., 1998; Pollock et al., 2018; Seccombe et al., 1985; Kimpton 2018).

2. GEOLOGICAL SETTING/BACKGROUND

KANMANTOO FORMATION

The formation of the Kanmantoo Group involved the rapid deposition of a turbiditic metasedimentary sequence of sandstone and mudstone protoliths (Jago et al., 2003; Haines et al. 1996). The present-day Kanmantoo Group is composed of 7km thick clastic metasedimentary sequence that experienced regional low-pressure (0.3–0.5 GPa) metamorphism due to the Delamerian Orogeny, triggered by convergent tectonism throughout the palaeo-Pacific margin of Gondwana and resulted in forming distinct widescale metamorphic zonation (Dymoke & Sandiford 1992; Sandiford et al., 1995; Turner et al., 2009). Economic deposits located in the Cambrian group consist of a variation of Cu-Au, Fe-S, and Pb-Zn-Ag-(Cu-Au) formations, the largest Cu-Au deposit being Kanmantoo deposit containing 43.5 megatons of Cu at 0.6% and 0.1g per ton of gold. Located within the Adelaide Geosyncline in South Eastern South Australia (Pollock et al., 2018) (see figure 1), Kanmantoo mineralization is characterized by stockwork-veining orebodies in the form of the Kavanagh and Emily Star orebodies, and mineralization parallel to the bedding in the form of the Nugent orebody (Pollock et al., 2018). Minerology of the mine is commonly associated with pyrrhotite, chalcopyrite, sphalerite and pyrite (Pollock et al., 2018).

The associated contractional Delamerian orogenesis that metamorphosed the sediments of the Kanmantoo group initiated at 514 Ma (+/- 3 Ma) and lasted 24 Ma until 490 Ma (+/- 3 Ma) (Foden et al., 2006). Orogenesis was terminated through the process of rapid uplift, followed by cooling and then extension in relation with post-tectonic magmatism (Foden et al., 2006). The Early Cambrian was fundamentally characterised by Eastern

Australia being in a state of extension, resulting in the opening of the Kanmantoo Basin and accompanying magmatism (Foden et al., 2006).

The Kanmantoo Cambrian Group extends throughout South Eastern South Australia and houses the Kanmantoo Cu-Au deposit. Speculation persists regarding the possibility of uncovering undiscovered mineralization in the area and as the Kanmantoo Cu-Au mine hosts the most pronounced mineralization in the area it will compose the samples analysed in this study.

Figure 1: Map of the Kanmantoo Cambrian Metasediment Group in relation to South Eastern South Australia. Trace of the Kanmantoo Cambrian Group formation adapted from (Jago et al., 2003).

ORE GENESIS CONTROVERSY

The genesis of the Kanmantoo deposit remains disputed, with theories ranging from syn-sedimentary to metamorphic and post-peak metamorphic models indicating varying degrees of remobilization of fluids (Oliver et al., 1998; Pollock et al., 2018; Seccombe et al., 1985). The Kanmantoo mine ore genesis is disputed in regards to the evidence

provided for a syngenetic (Pollock et al., 2018; Seccombe et al., 1985), or an epigenetic origin (Oliver et al., 1998, Parker, 1986; Thomson 1975). The proposed syngenetic theory favours a sedimentary exhalative origin of base metal mineralization through subsurface copper and sea-floor lead-zinc accumulation by the circulation of hydrothermal fluids (Pollock et al., 2018; Seccombe et al., 1985), however the epigenetic models favours peak to post-peak metamorphic conditions creating mineralization as a result of the interactions between metamorphic and synorogenic hydrothermal fluids and the significant changes in bulk chemistry caused as a result of fluid infiltration (Oliver et al., 1998).

I-S ISOTOPIC SIGNATURES

Existing literature regarding, I-type, S-type and A-type Delamerian granites are fundamental in assessing the correlation of isotopic signatures with the timing of events and consequent formation of mineral deposits (Foden et al., 2002; Hammerli et al., 2014). Previous detrital zircon age data (Gibson & Ireland 1996) and low 143Nd/144Nd isotopic ratios (Foden et al., 2002; Hammerli et al., 2014) indicates the Kanmantoo group to be a Precambrian continental sediment source. Understanding the formation of an ore deposit requires knowledge of the sources of fluids and metals and is essential to progressing future exploration of precious metals (Robb, 2005). Isotopic datasets on the Delamerian deposits in South Australia increase the understanding of source material required to constraint the deposits by identifying the timing of granitic and orogenic events (Richards, 2013; Foden et al., 2002; Foden et al., 2006). Characterising the mineralization of the Kanmantoo Cu-Au deposit to be deemed an igneous deposit would indicate the mineralization could have derived from a potential array of mantle sources

(Richards, 2011) and recognizes an I-type isotopic signature. The mineraology of the deposit created from the magma is then determined by the quantity of chalcophile and siderophile metals present within the magma derived from the source (Richards, 2011). When deciphering the formation of the Kanmantoo Cu-Au deposit the presence of a sedimentary protolith will determine that mineralization associated with an ore-bearing fluid was the product of an S-type granitic signature, indicating a scenario where the partial melting of supracrustal rocks in a continental arc, continental collision or post-orogenic uplift and collapse settings has occurred (Chappell & White 2001; Pollock et al., 2018). A lack of mantle input will indicate that the mineralization in the deposit is formed by an influx of hydrothermal fluids and a modification or replacement of the host (Pollock et al., 2018; Seccombe et al., 1985).

3. SAMPLE COLLECTION

Table 1: Chart of the Kanmantoo mine samples, geological group, and location. Samples are a combination of new samples provided by Hillgrove Resources and legacy samples from Kimpton 2018 and Morgan 2019. Coordinates were taken in Adelaide Hills UTM zone 54H

Sample	Group	Type	Source of Sample + Data	Easting	Northing	Ages (Kimpton 2018; Morgan 2019)
Kanmantoo 1	**Host rock**	Regional host rock within mineralization sequence	Powders, and WR data created	317988	6114135	KMT1 (Thin section proximal equivalent) (496.98±2.18 Ma)
Kanmantoo 2	**Host rock**	Regional host rock within mineralization sequence	Powders and WR data created	317988	6114135	KMT1 (Thin section proximal equivalent) (496.98±2.18 Ma)
Kanmantoo 3	**Host rock**	Regional Host rock distal to mineralization sequence	Powders, and WR data created	318628	6114361	BKDK1 (Thin section Distal equivalent) (499.09±1.54 Ma)
Kanmantoo 4	**Host rock**	Regional Host rock distal to mineralization sequence	Powders, and WR data created	318628	6114361	BKDK1 (Thin section Distal equivalent) (499.09±1.54 Ma)
Bk25	**Hydrothermal**	Vein with chalcopyrite mineralization	(Kimpton 2018) – New powder made for Sr-Nd	318326.8E	6114809N	485.35 ± 2.46 Ma
Fule	**Hydrothermal**	Vein - Aluminous segregation	(Kimpton 2018) – New powders made for Sr-Nd	318100	6114847	BKBDG2 (Aluminous segregation equivalent) (498.6 + 16.7 Ma)
Albitite (Referred to as KM2-STH-G)	**Hydrothermal**	Felsic Crystalline rock -Extremely altered	(Morgan 2019) – New powders made for Sr-Nd	317469.87	6113094.47	
Petwood Granite (Referred to as the KM2-HWY-G)	**Granite**	Granite located near town of Petwood	(Morgan 2019) – New powders made for Sr-Nd	313804.34	6115444.03	
Sawpit Granite (Referred to as the DAW-SYN)	**Granite**	Granite located 7km north-west of Kanmantoo	(Morgan 2019) – New powders made for Sr-Nd	315816.16	6120088.00	501.0 ± 58 Ma
Thomas Granite	**Granite**	Granite located south of Kanmantoo	Powders, and WR data created	317321	6112723	

Prior to analysis the collection of 8 samples was undertaken at the Kanmantoo Mine Tenement located 52km South East of Adelaide. The samples consisted of hand samples, thin sections, and powders. Samples acquired from Hillgrove consisted of Brayden Morgan's 2019 and Ben Kimpton's 2018's previous work composing the Albitite, Fule, BK25, Sawpit, Petwood granite and Thomas granite. 4 additional samples were collected from the surface of McFarlane's Hill, separated into the proximal Kanmantoo 1-2 representing the edge of the mineralization sequence, and Kanmantoo 3-4 located distal to the edge of the mineralization sequence (see figure 2). Samples have been separated into three groups composing granitic, hydrothermal, and regional host rocks, indicative of the characteristics observed from the hand samples and previous findings to determine their association with the genesis of the Kanmantoo mineralization.

Figure 2: Geographic Image of Kanmantoo Mine in relation to granitic (orange), hydrothermal (red) and regional host rock (blue) samples.

4. METHODOLOGY

4.1. Sr-Nd Isotope Preparation

Sr-Nd isotope analysis consisted of column chemistry preparation at the University of Adelaide Clean labs and fusing Sr-Nd concentrate on filaments to be placed in the Thermal Ionization Mass Spectrometer. The sample set composes the 8 samples studied in this thesis and the addition of a standard BHVO-2 and Blank-2628 (see table 3). Sample pulps were individually weighed out at 0.1g and placed in a labelled teflon container. Samples were then subject to acid digestion by dissolving the samples in a solution of HNO_3 or HCL and heating on a hot plate until complete decomposition of the matrix. Samples ran through a centrifuge to identify remaining organics and acid digestion was repeated if necessary. Samples were separated into individual Sr and Nd containers and dissolved in an appropriate solvent. The samples were loaded into separate columns and passed through a specific Sr or Nd resin to isolate the trace element within the sample. Elemental concentrates were dissolved in specific solutions and fused onto a heated filament to be loaded onto the thermal ionization mass spectrometer and analysed by lab technicians at the University of Adelaide.

The standard measured alongside the samples studied in the thesis (BHVO-2) generated results within the Georem preferred values (Jochum et al. 2016) for Hawaiian Basalt BHVO-2 rock standards of 0.512939 +/- 0.000014 $^{143}Nd/^{144}Nd$ and 0.703478 +/- 0.000034 $^{87}Sr/^{86}Sr$ (See table 2).

4.2. Whole Rock Geochemistry

Whole rock analysis consisted of x-ray fluorescence (XRF) and ICP-AES analysis at ALS laboratories. BK25 samples were powered and made into fused disks, where major elemental analysis was conducted using ICP-AES and transition metal and trace elemental analysis was conducted by ICP-MS 38 major element fusion. Remaining Kanmantoo mine samples conducted major elemental analysis through measuring x-ray fluorescence emitted by elements within the sample using XRF-26 analysis and employing ICP-MS to measure transition metal and trace element analysis.

4.3. Petrography

Hand sample petrography consisted of the identification of fist-sized hand samples under a hand lens and distinguishing observations regarding minerology, texture, colour, foliation, deformation and hydrothermal or magmatic input. Thin section petrography was conducted at the University of Adelaide using a Leica DM2700 P microscope to observe 7 polished thin sections. The KMT-1 and BKDK1 thin sections from Ben Kimpton and Brayden Morgan's previous thesis were analysed under different regional host rock alias's, of which KMT1 represents a host rock proximal to mineralization and BKDK1 a host rock distal to the mineralization. Reflect light was employed for the hydrothermal BK25. Sample specific screen captures were taken for

analysis so that observations and interpretations regarding the genesis of the samples could be determined.

5. RESULTS

5.1. Hand Sample Petrography: Hydrothermal Group

Sample BK25, Fule, Albitite:

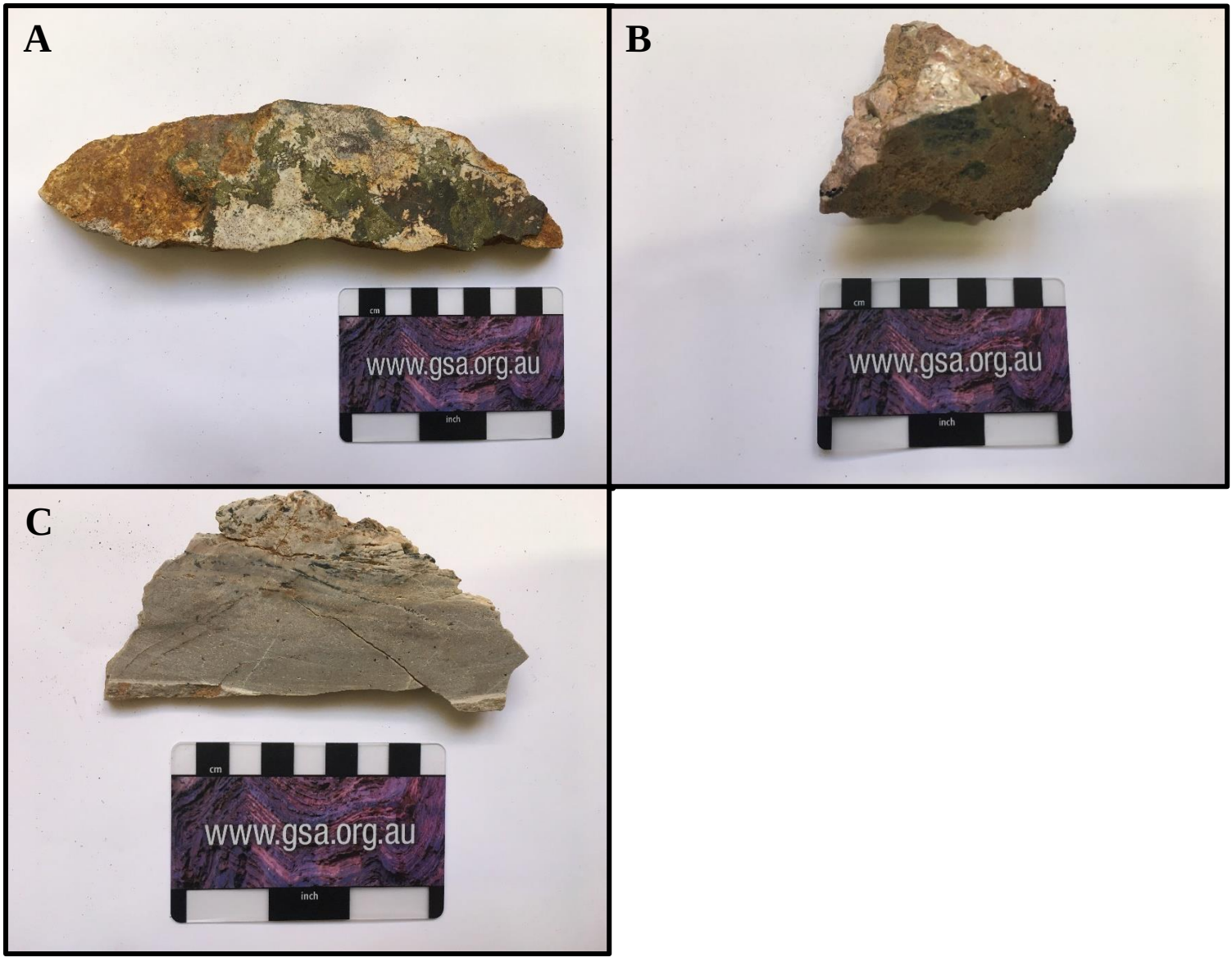

Figure 3: Photography of hand samples allocated to the Hydrothermal group hand located within the Kanmantoo Mine tenement. A) Kanmantoo Mine BK25 hydrothermal hand sample B) Kanmantoo Mine Fule Aluminous Vein and C) Albitite hydrothermal hand samples. Photography taken without flash in ambient lighting with scale attached.

5.2. Hand Sample Petrography: Host Rock Group

Sample Kanmantoo1, Kanmantoo 4:

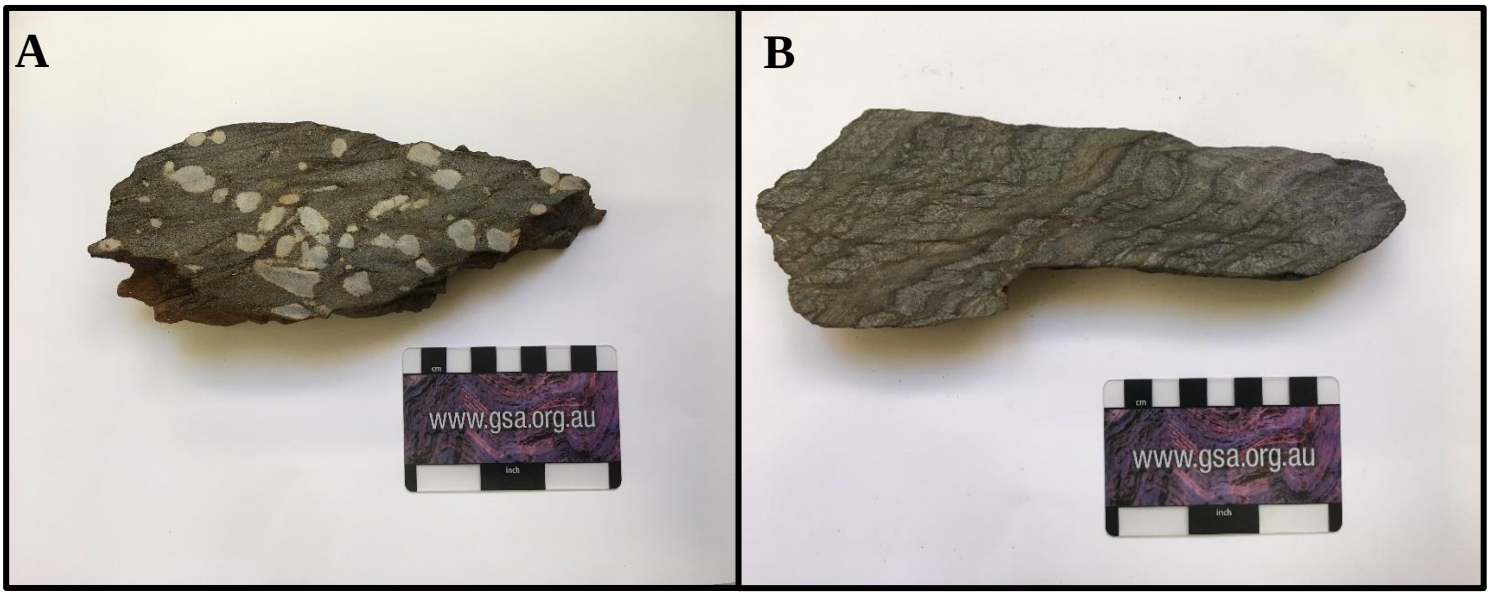

Figure 4: Photography of hand samples allocated as Regional Host rocks taken as surface grabs within the Kanmantoo Mine tenement. A) Kanmantoo 1 proximal regional host rock hand sample and B) Kanmantoo 4 distal regional host rock hand sample.

5.3. Hand Sample Petrography: Granite Group

Sample Sawpit Granite, Thomas Granite

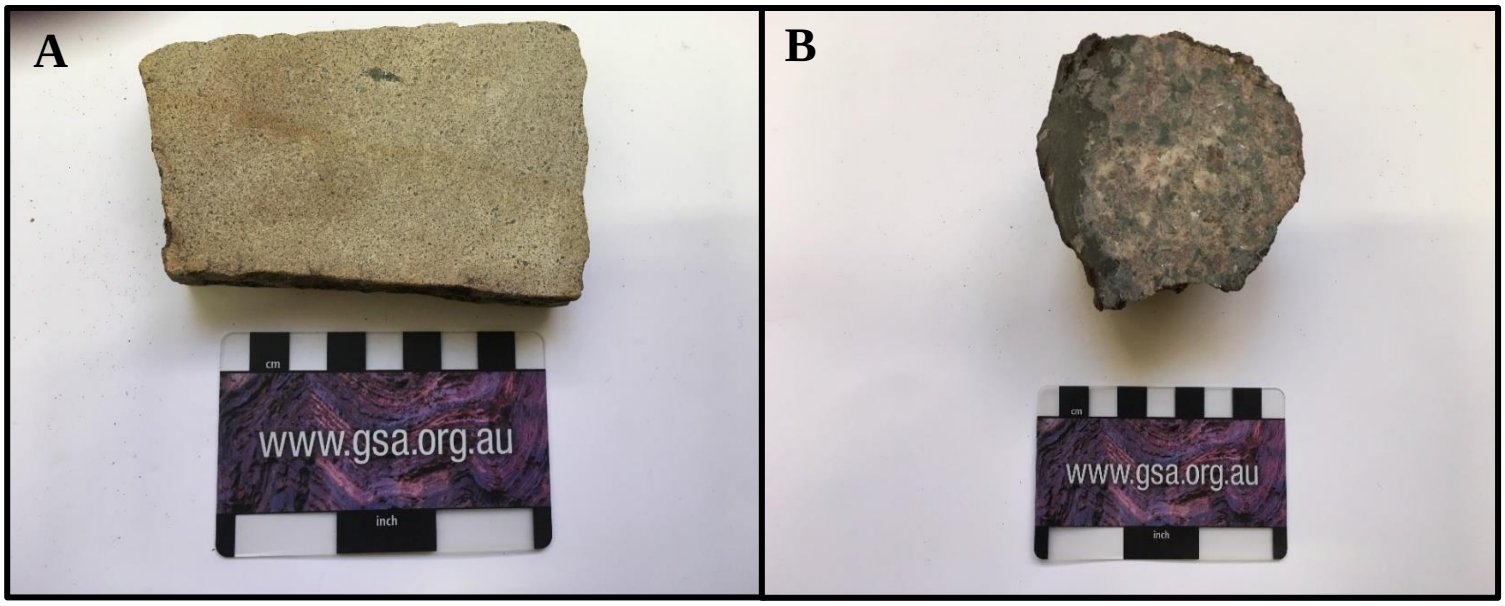

Figure 5: Photography of hand samples allocated to the granite group located within a nearby vicinity to the Kanmantoo Mine tenement. A) Sawpit granite (Commonly referred to as Daw-Syn) hand sample and B) Thomas granite hand sample. The Petwood Granite hand sample is allocated to the granitic group however was unavailable to be sampled due to inability to contact the rightful landowners

5.4. Thin Section Petrography: Hydrothermal Group

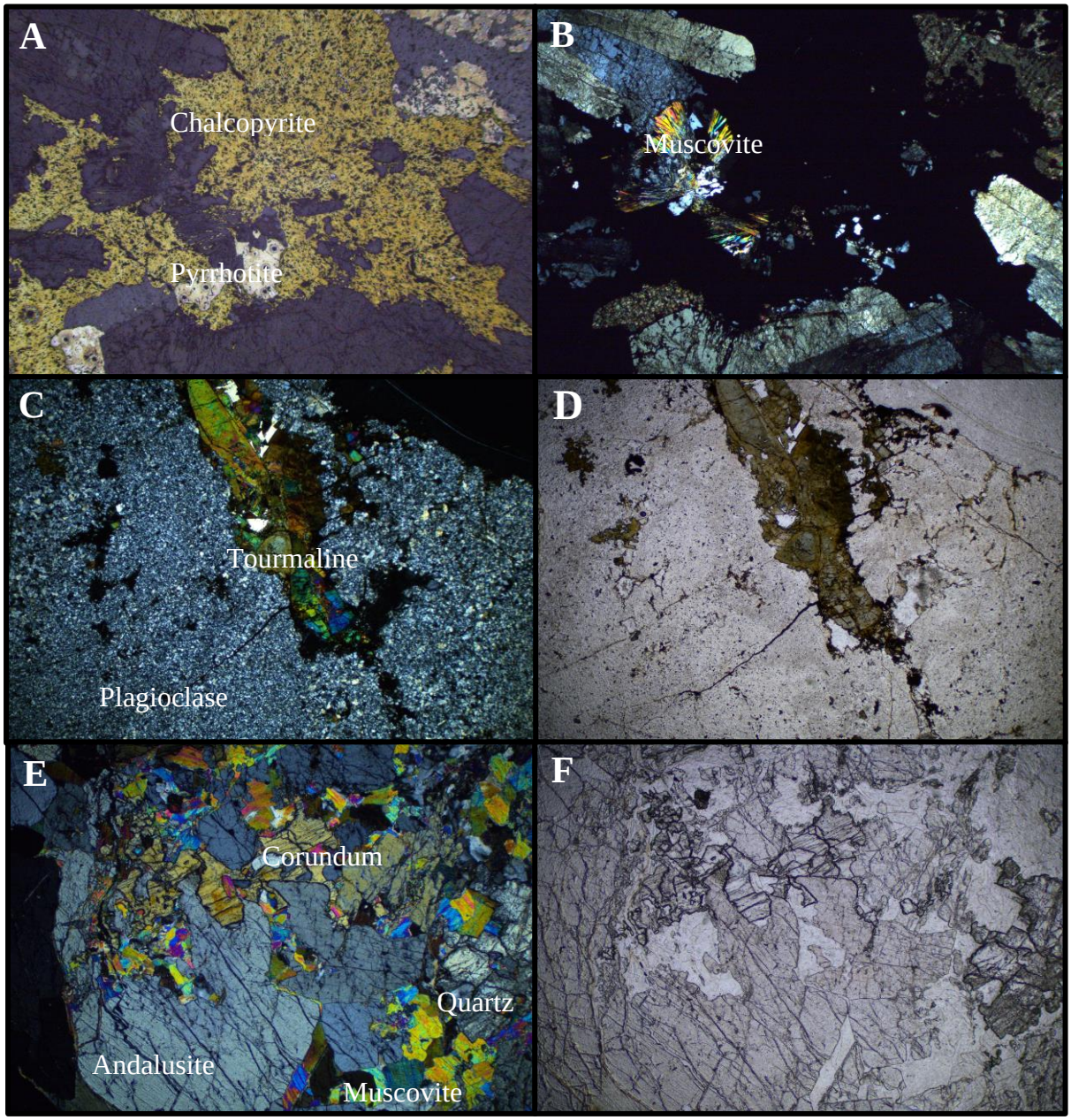

Figure 6: Thin Section Screen captures of the hydrothermal Kanmantoo Mine thin sections. A) Hydrothermal thin section BK25A indicating mineralization in reflected light, B) Hydrothermal thin section BK25A in cross polarised light, C) Hydrothermal thin section KM2-Sth-g (Albitite) in cross polarised light, D) Hydrothermal thin section KM2-Sth-g (Albitite) in plain polarised light, E) Aluminous vein Fule in cross polarized light and F) Aluminous vein Fule in plane polarised light. Microscopy was undertaken on a lens magnification of 1.6 X 0.005.

5.4.1. Hydrothermal Group Observations

Sample BK25: At the hand sample scale observations (see figure 3) consist of 20% sulphide infilling 0.5-1.5cm wide veins, composed of chalcopyrite (15 wt. %) and pyrrhotite (5 wt. %) and the remaining sample composing 45% plagioclase, 25% K-feldspar and 10% quartz. The veins are chalcopyrite dominated and persist throughout the entirety of the hand sample and have no indistinguishable grain size or crystal structure. The quartz, plagioclase and k-feldspar have a grain size of between (125-150um). Thin section petrography remains consistent with hand sample petrography yet enables observation of biotite, muscovite, and foliation of the country rock. Furthermore, the thin section scale depicts the presence of sulphide infill and a large chalcopyrite cross-cutting veins dominating the hydrothermal mineralized sample BK25 throughout the length of the specific thin section and observations of the specific sample remain consist under the microscope with 30% plagioclase, 10% k-feldspar, 15% quartz, 5% muscovite, 5% biotite, 25% chalcopyrite and 10% pyrrhotite. Under the thin section the plagioclase shows dominant 20um grain sizes and is often bordered by muscovite as pictured in (see figure 6), or by low relief quartz or k-feldspar. The sample predominantly consists of sulphides infilling empty spaces adjacent pronounced plagioclase and muscovite crystals. The veins consist of yellow-orange chalcopyrite (80%) and pale-yellow pyrrhotite (20%) and crosscut the thin section. In areas not dominated by vein assemblages, biotite wraps around the muscovite and defines the foliation in a similar yet less defined manner to that of KMT1 and BKDK1 regional host rocks.

Sample Fule: At the hand sample scale (see figure 3) this sample is massive and unlayered, with mineral observations consisting of biotite (30%), muscovite (30%), and andalusite (40%). Sample colouration appears to have an orange-black weathered appearance that is found sporadically throughout the xhand sample. The biotite has a transparent clear colour and variable sizes, ranging from 0.2 to 1cm in size and appearing in square sheets. Quartz grains are indistinguishable and estimated to be approx. (50um). The muscovite appears to bend or fold around the quartz grains and muscovite is located adjacent the biotite. At the thin section scale observations of the Aus-7 (Fule) sample (see figure 6) are consistent with observed hand sample petrography and clearly introduces evidence of corundum and quartz. Observations consist of an andalusite (40%), muscovite (20%), quartz (13%), corundum-abundant (25%) thin section with small quantities of biotite (2%). Andalusite is the prominent mineral in the sample, encompassing areas in-between alternate mineral grains and composing the matrix. The matrix of the sample appears fractured and infilled with corundum, muscovite, and biotite, with corundum and muscovite occasionally appearing disseminated. Quartz borders muscovite and the corundum appears to have a rough texture, most likely a result of the hardness of the material and polishing of the thin section. Muscovite crystals bend or fold around the corundum grains and crystalize along the outskirts of the crystal’s rims.

Sample Albitite (KM2-STH-G): At the hand sample scale observations consists of biotite (15%), muscovite (15%), and a white albite groundmass (70%), that is cross-cut by 1-3mm wide black streaks composed of biotite present throughout the sample (see figure 3). The white albite groundmass has an indistinguishable grain size. Grain sizes in the hand sample vary with muscovite reaching 5mm and biotite of a 3mm grain size. The thin section confirms the presence of the plagioclase end member albite by containing predominantly plagioclase and minor amounts of tourmaline. At the thin section scale observations consists of tourmaline (15%), biotite (7%), muscovite (3%) and plagioclase (75%) (see figure 6). The large tourmaline crystal displayed has a 60um length and 20um diameter (see figure 6). Plagioclase composes the bulk of space adjacent either side of the tourmaline crystals. The tourmaline crystal appears as if it cross-cut and infilled empty space present in a predominantly plagioclase rock. The thin section depicts complete replacement of the host schist by albite and minor quantities of tourmaline. Relict layering is evident, but the minerology of the host rock has been entirely replaced.

5.5. Thin Section Petrography: Host rock Group

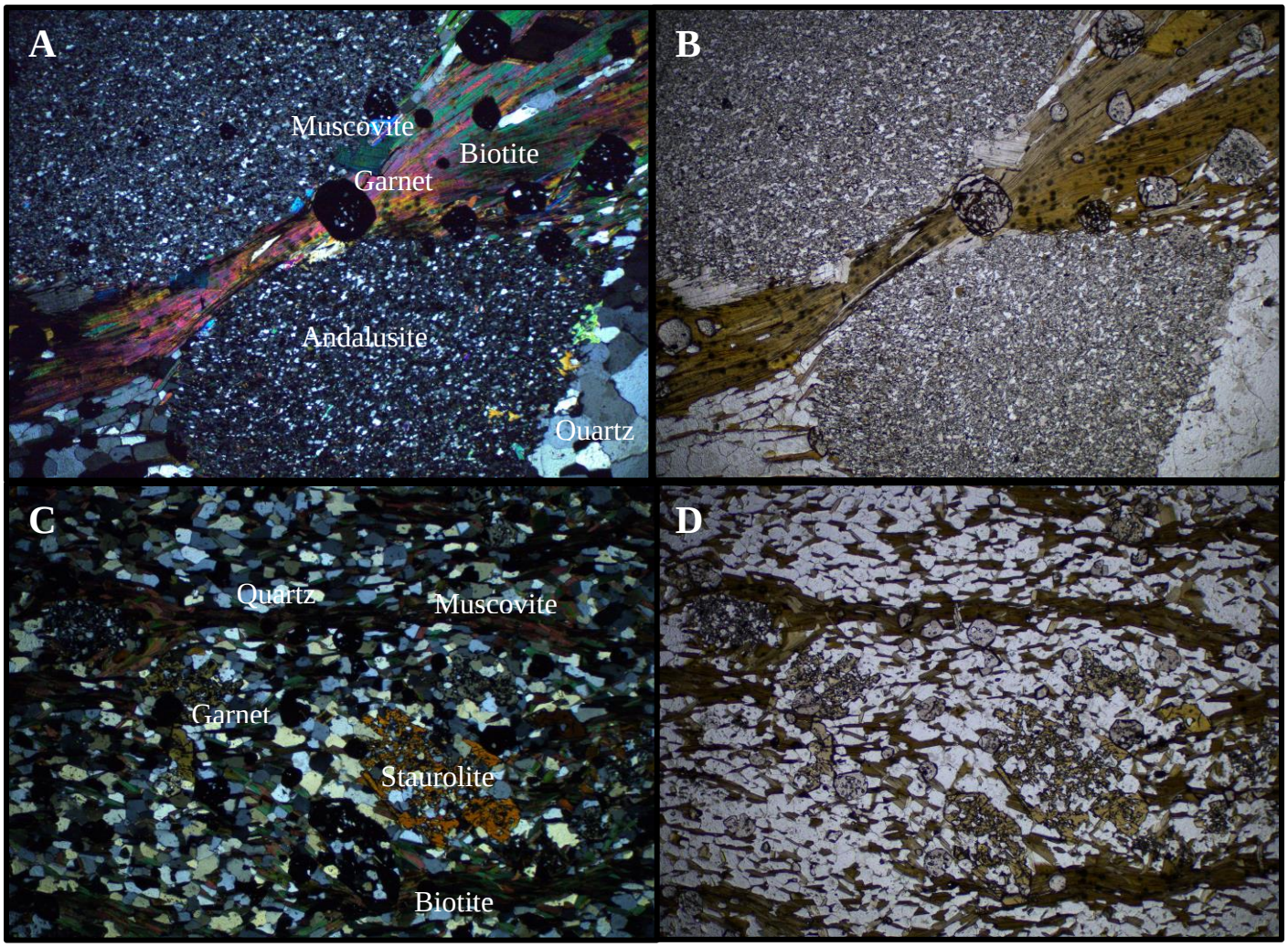

Figure 7: Thin Section Screen captures of the regional host rock thin sections located on the outskirts of the Kanmantoo mine. The thin sections depict; A) KMT-1 proximal regional host rock in cross polarised light, B) KMT-1 proximal regional host rock in plane polarised light, C) BKDK1 distal regional host rock in cross polarised light and D) BKDK1 distal regional host rock in plane polarised light. Microscopy was undertaken on a lens magnification of 1.6 X 0.005.

5.5.1 Host Rock Group Observations

Sample Kanmantoo 1: At the hand sample scale observations (see figure 4) consist of a fine-grained (150 -250um) silver-grey groundmass, containing mica, with 0.5cm-2cm wide white-grey andalusite porphyroblasts. The foliation wraps around the andalusite grains in a dextral motion and appears in dark-grey banding. Strong deformation is present throughout the hand sample, affecting both the porphyroblasts and matrix. The hand sample is estimated to be composted of 30% andalusite crystals and 70% a dark brown to silver matrix. At the Thin Section scale observations of Sample KMT-1 observe the relationship between the minerals that compose the foliation and the garnet porphyroblasts that crosscuts it (see figure 7). Observations consist of identifying the minerals muscovite (5%), garnet (15%), quartz (20%), poikiloblastic andalusite (45%) and biotite (15%). Muscovite is present in small quantities and located adjacent the biotite. There is foliation present which is predominantly composed of biotite. Muscovite and biotite define the foliation. The foliation intersects the andalusite, andalusite forms around the foliation and 40um black garnet porphyroblasts crosscut the foliation (see figure 7). Andalusite appears to infill in the empty spaces adjacent the foliation and is generally boarded by quartz.

Sample Kanmantoo 4: At the hand sample scale observations consist of 1-2cm wide grey-metallic coloured bands that appear orthogonal to the bedding (see figure 4), characterised by silver micaceous rims. The sample contains primary sedimentary bedding and a high angle metamorphic foliation defined by mica. The sedimentary bedding appears to be composed of entirely quartz and the bands dominated by biotite. The foliation is present throughout the entire hand sample. Foliation is heavily defined,

and the bedding appear homogenous. The rock appears to be composed of 30% biotite and 70% quartz. At the Thin section scale Sample BKDK-1 observations identify the individual minerals present within the foliation and banding. Observation consisting of quartz (50%), muscovite (3%), garnet (15%), staurolite (12%) and biotite (20%). Muscovite and biotite define the foliation, of which is predominantly composed of biotite. The fabric partially wraps the staurolite (see figure 7). Garnet tends to crosscut the quartz and biotite however is generally located outside the biotite-muscovite foliation. Biotite and quartz form the bulk of the sample and appear to form an interwoven texture. Poikiloblastic Staurolite of 20-40um size is present throughout the thin section.

5.6. Thin Section Petrography: Granite Group

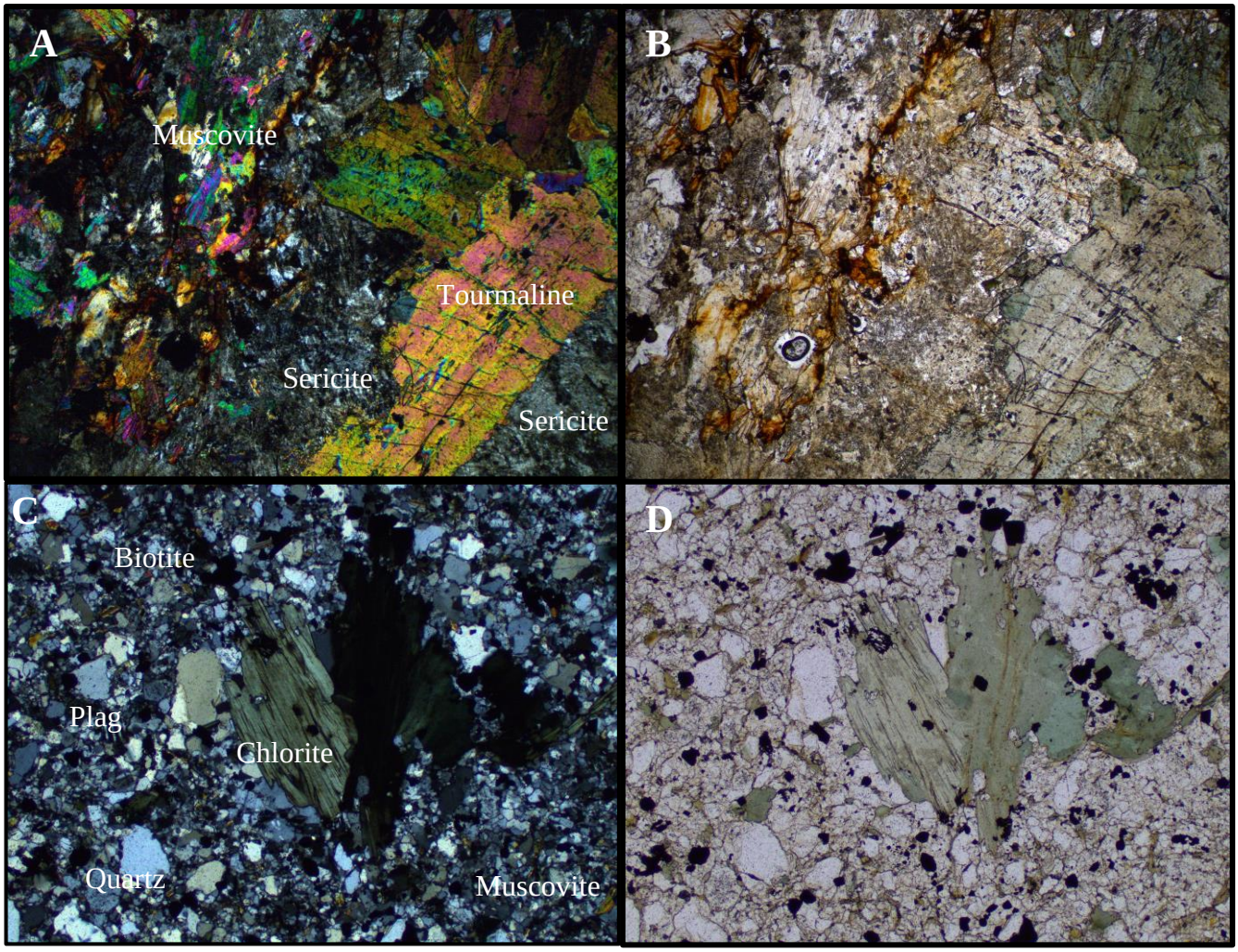

Figure 8: Thin Section Screen captures of the granite group thin sections located near the Kanmantoo mine. A) KM2-HWY (Petwood Granite) thin section in cross polarised light, B) KM2-HWY thin section in plane polarised light, C) Daw-Syn (Sawpit Granite) thin section in cross polarised light and D) Daw-Syn thin section in plain polarised light. No thin section was created from the Thomas granite hand sample. Microscopy was undertaken on a lens magnificent of 1.6 X 0.005 for figure A) and figure B) and on a lens magnification of 2.5 X 0.007 for Figure C) and Figure D).

5.6.1 Granite Group Observations

Sample Sawpit Granite (Daw-Syn): At the hand sample scale observations consist of quartz (55%), plagioclase (30%), chlorite (5%) and oxides (10%) (see figure 5). The sample has an aphanitic texture and has grain sizes of (1mm). Chlorite is present as a (1cm) size grain in the upper-centre location of the hand sample. At the thin section scale observations of Sample Daw-Syn identify distinct chlorite crystals at different stages of extinction (see figure 8). Minerology consists of chlorite (20%), quartz (50%), plagioclase (15%), biotite (5%) and muscovite (5%), with approx. (10%) opaques present throughout the sample. Chlorite is present in 40um grains and is pictured above in two parallel grains in opposite stages of extinction (see figure 8) and is spread throughout the sample varying grain sizes. The sample is observed to have poorly defined edges, most easily observed in plane polarized light. The matrix of the sample is composed of predominantly quartz and to a lesser extent plagioclase. The sample has anomalously small grain sizes within the matrix in comparison to other Kanmantoo mine samples, with many grains <10um. Biotite and muscovite are dispersed unevenly throughout the sample and display no clear foliation.

Sample Thomas Granite: At the hand sample scale observations consist of quartz (30%), potassium feldspar (30%), plagioclase (15%), biotite (15%) and muscovite (10%). The Thomas granite is observed to possess more dark-coloured biotite and plagioclase minerals than other Kanmantoo group counterparts. The muscovite appears as pink (5mm) size grains and the biotite appears as dark brown (6mm) sized grains. The potassium feldspar has the largest grain size at (0.5-1cm), of which plagioclase appears to be intergrown or had grown adjacent the potassium feldspar crystals. The sample has defined crystal sizes and a characteristic coarse igneous texture. Sample appears moderately more mafic than other Kanmantoo granitic samples.

Sample Petwood Granite (KM2-HWY): At the thin section scale observations consist of sericite (45%), muscovite (25%), tourmaline (15%) and (15%) biotite. The k-feldspar appears low-relief and of indistinguishable grain size and has been almost completely replaced in some places by sericite, however relict remains still exist (see figure 8). Tourmaline crystal observed with 60um diameter and is encased adjacent sericite alteration. Muscovite and biotite have disjointed grain sizes and appear adjacent the sericite alteration but not tourmaline. Muscovite and biotite grain size is variable, and texture is often indistinguishable (see figure 8). The tourmaline is highly pleochroic and can form crystals 200um in length.

5.7. GEOCHEMISTRY OF MAJOR ELEMENTS

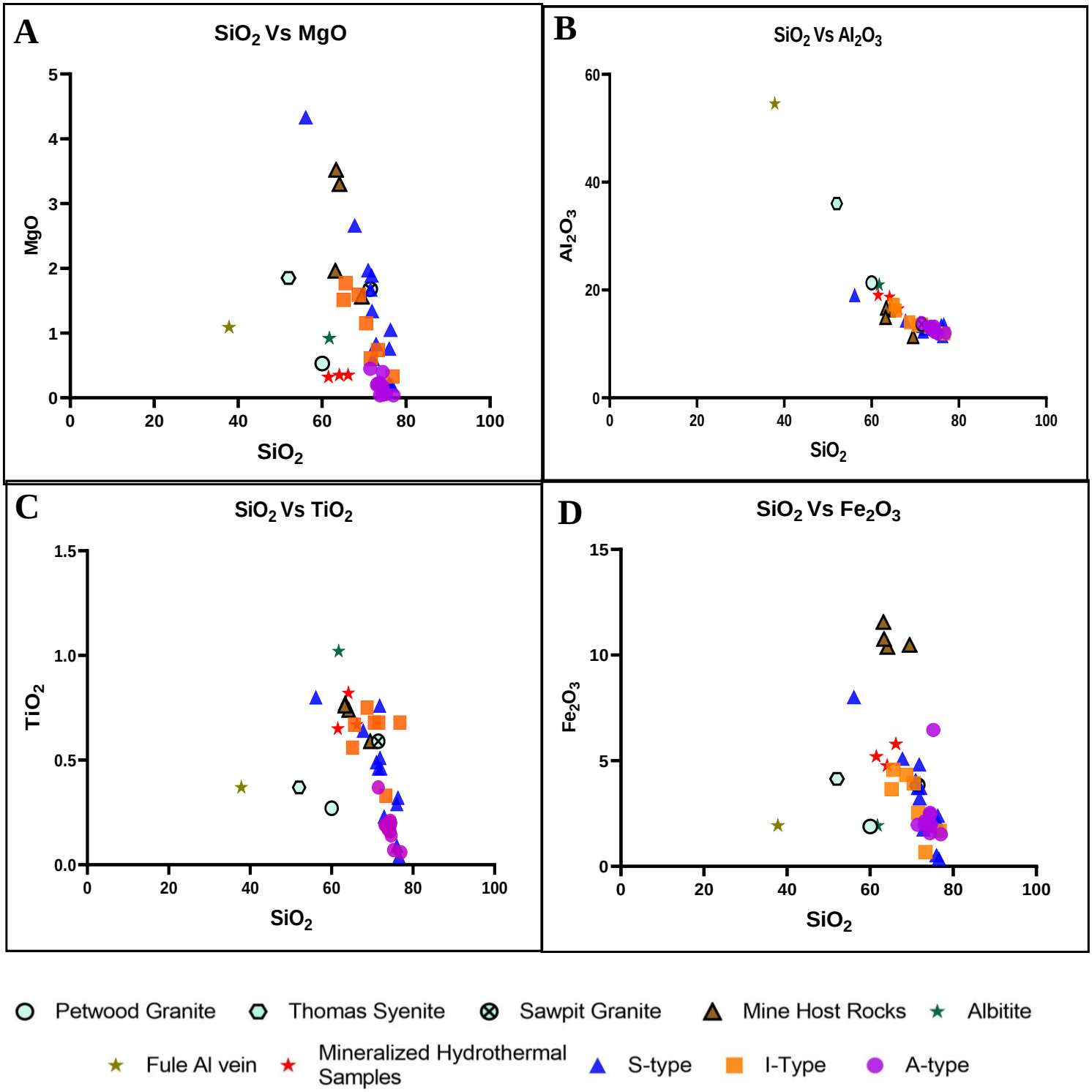

Figure 9: Geochemical plots of major elements against SiO_2. The samples from this study are compared with the Delamerian granites from Foden et al., 2002 and Foden et al., 2020 (Foden et al., 2002; Foden et al., 2020).

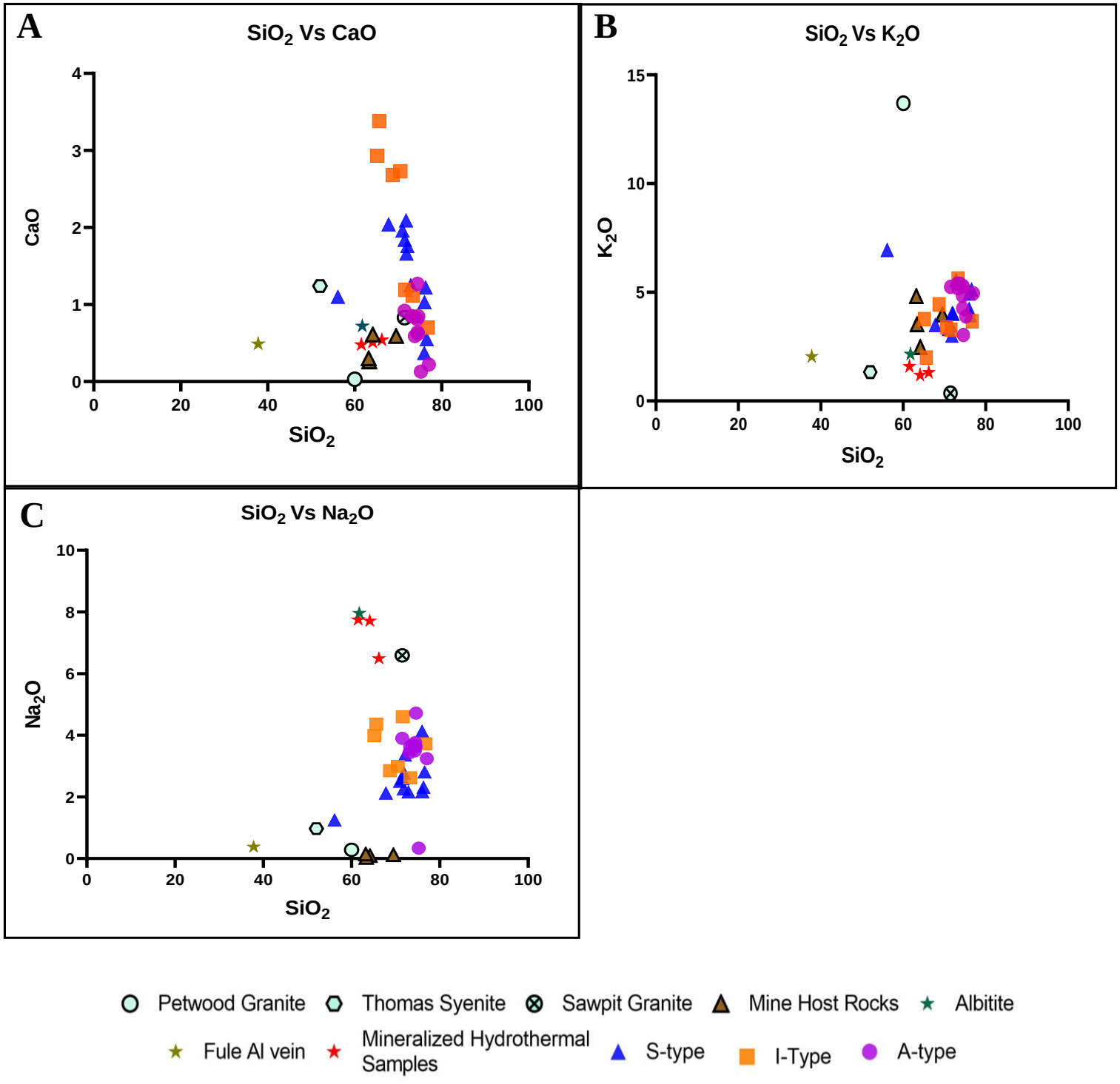

Figure 10: Continuation of geochemical plots of major elements against SiO_2. The samples from this study are compared with the Delamerian granites from Foden et al., 2002 and Foden et al., 2020 (Foden et al., 2002; Foden et al., 2020).

5.8. Whole Rock Transition Metal Geochemistry

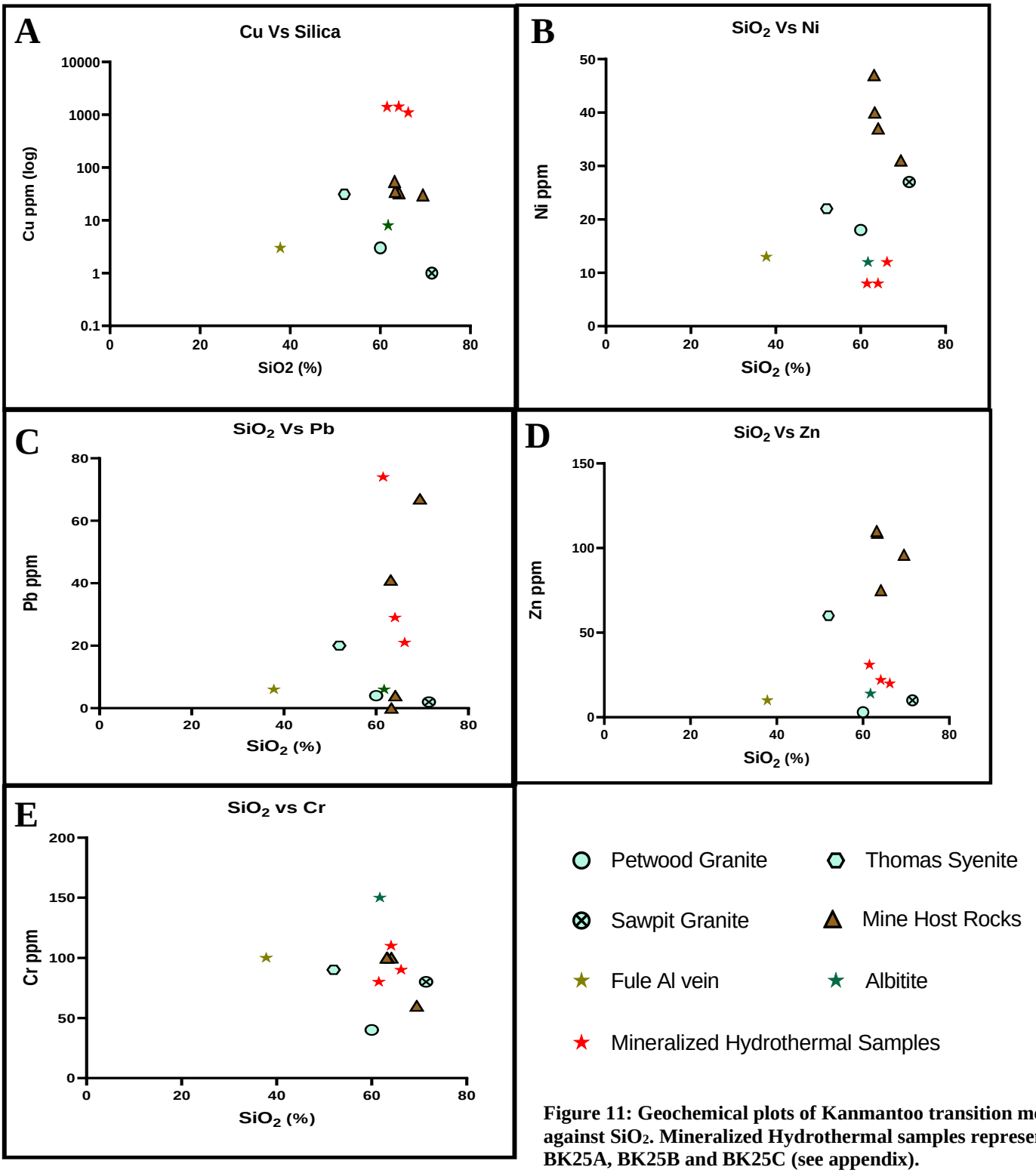

Figure 11: Geochemical plots of Kanmantoo transition metals against SiO_2. Mineralized Hydrothermal samples represent BK25A, BK25B and BK25C (see appendix).

5.9. Hydrothermal Samples Normalised to Host Rocks

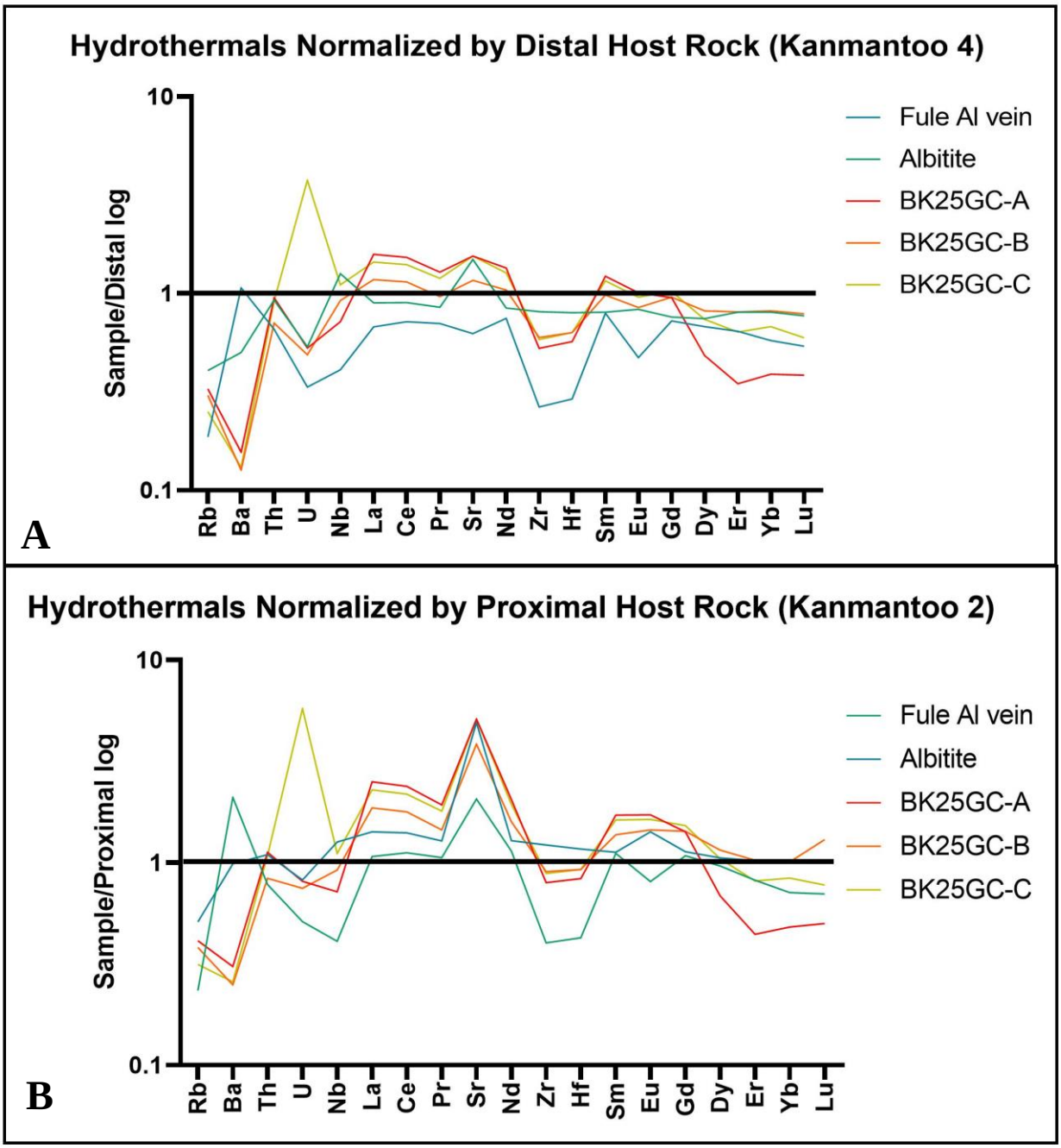

Figure 12: **Trace element plot of hydrothermal group samples normalized to regional host rock group. The samples from the hydrothermal group are compared against the host rocks to determine the flux of elements introduced through fluids.**

5.10. Trace Element Data Spider Diagrams

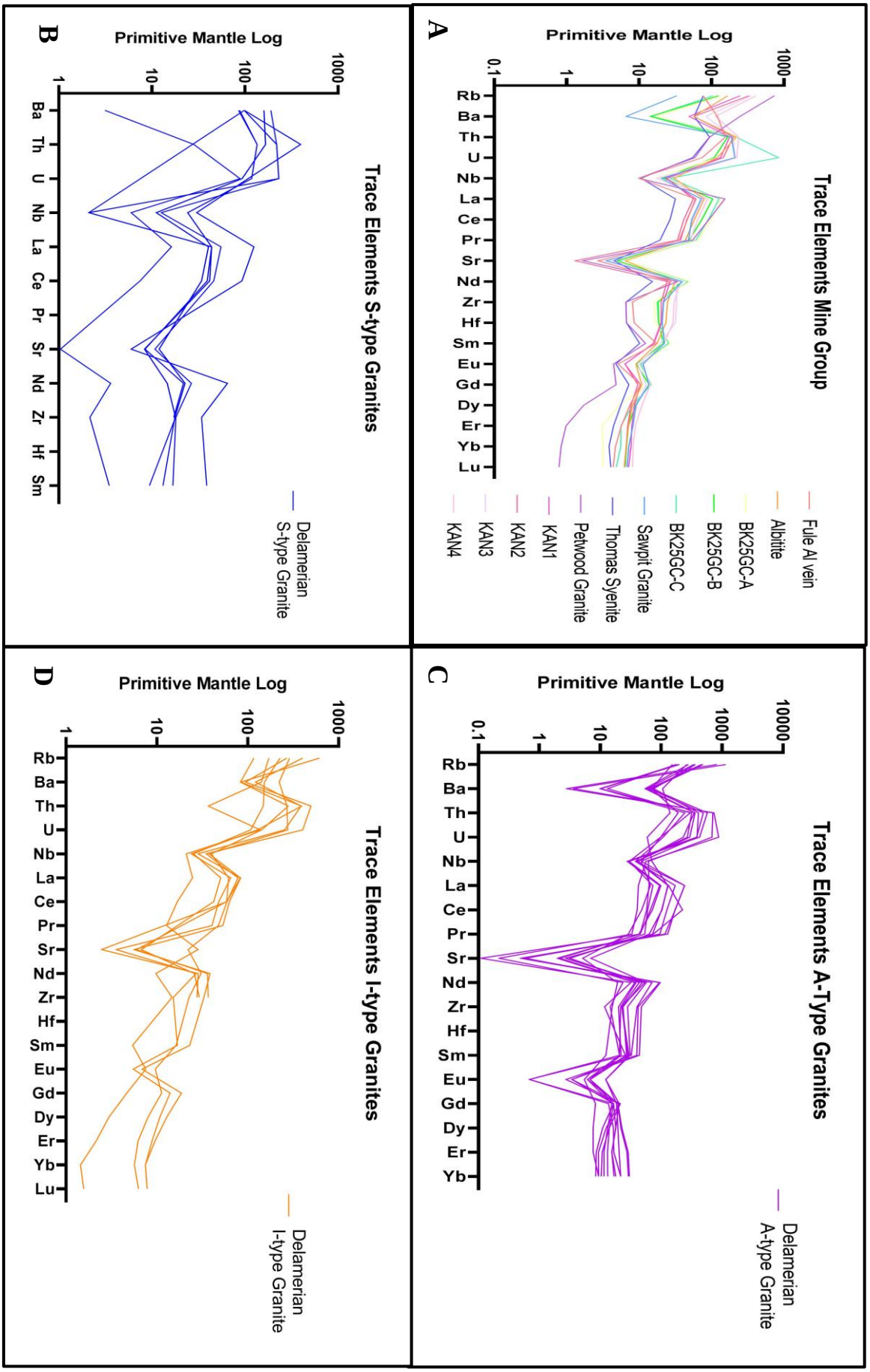

Figure 13 : Spider diagrams comparing the enrichment or depletion of trace elements composing the samples investigated in this study. The samples from the study are compared with Delamerian I, S and A-type granite trace element data from Foden et al., 2002 and Foden et al., 2020 (Foden et al., 2002; Foden et al., 2020)

5.11. $^{143}Nd/^{144}Nd$ and $^{87}Sr/^{86}Sr$ Isotope Standard Error Results

Geological Reference Material and Error Percentage (%)

Table 2: **BHVO-2 Hawaiian Basalt Standard (Georem 2020) indicated an $^{87}Sr/^{86}Sr$ percentage error of 0.001842% from the published value compared to the experimental value gathered in this thesis (Jochum et al. 2016). The BHVO-2 Hawaiian Basalt indicated an $^{143}Nd/^{144}Nd$ percentage error of 0.000278% from the published value compared to the experimental value gathered in the thesis (Jochum et al. 2016).**

	87Sr/86Sr	Mean	143Nd/144Nd	Mean
BHVO-2 # 97 Experimental Value	0.703491	.000003	0.512978	1.90E-06
BHVO-2 Georem Value	0.703478	0.000034	0.512969	0.000014
Percentage Error (%)	0.001842		0.000278	

5.12. $^{143}Nd/^{144}Nd$ Vs $^{87}Sr/^{86}Sr$ Isotopic Composition

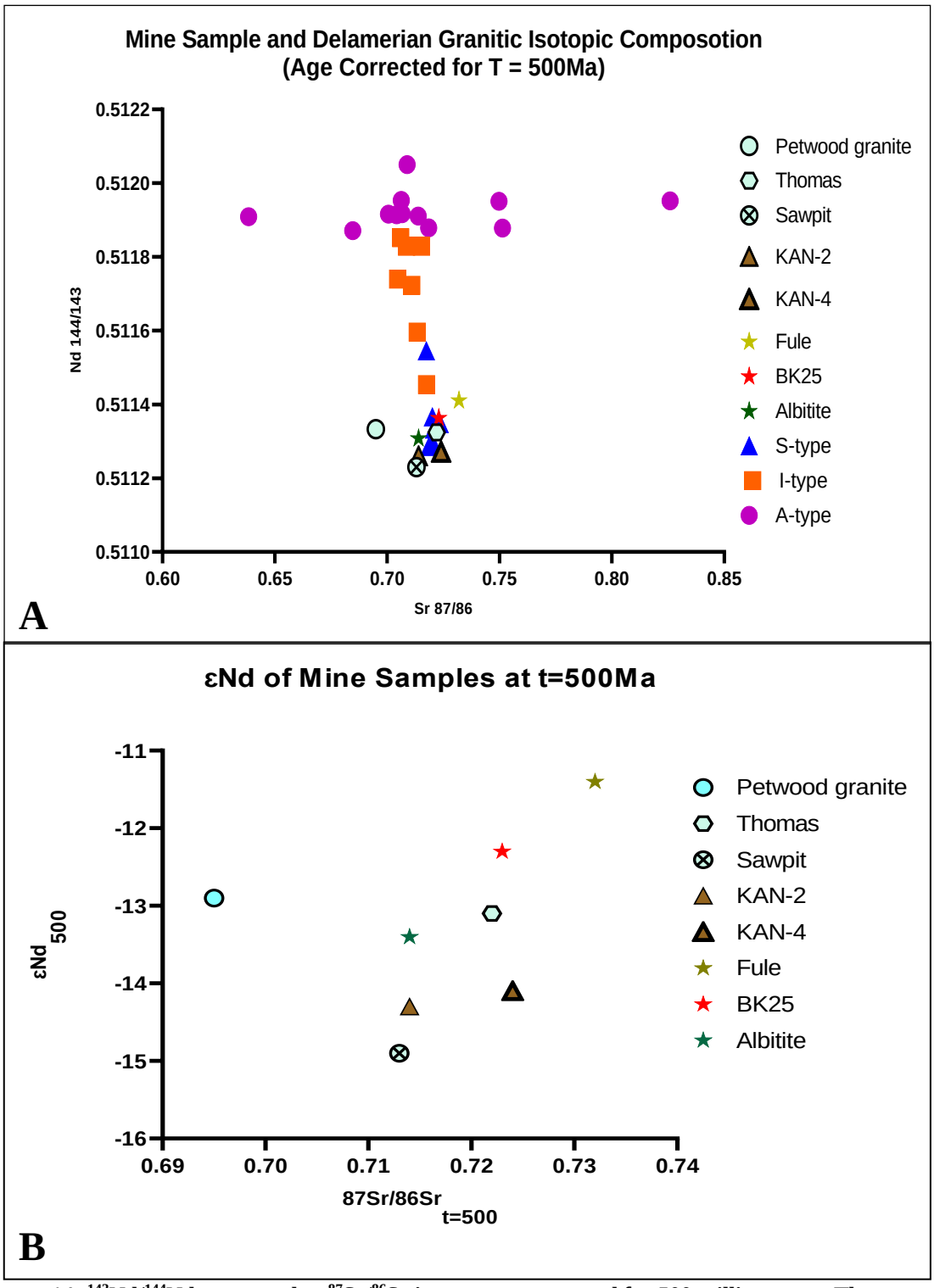

Figure 14: $^{143}Nd/^{144}Nd$ compared to $^{87}Sr/^{86}Sr$ isotope age corrected for 500 million years. The samples from this study are compared with the Delamerian granite isotopic data from Foden et al., 2002 and Foden et al., 2020 (Foden et al., 2002; Foden et al., 2020). Error bars are too small to be displayed as $^{87}Sr/^{86}Sr$ percentage error of the mine samples studied in this thesis is 0.001842% and the $^{143}Nd/^{144}Nd$ percentage error of the mine samples studied in the thesis is 0.000278%.

5.16. Geochemistry Results

Hydrothermal Group

The hydrothermal group is composed of the BK25-A, BK25-B, BK25-C, Fule and Albitite samples. The Al_2O_3 values range from 16.5-54.23% throughout the hydrothermal group, with the BK25 samples varying 16.5-19.05% and the Fule aluminous vein containing the highest Al_2O_3 concentration at 54.23%. The hydrothermal samples indicate similar concentrations of CaO residing within a common range of 0.48-0.72%. Fe_2O_3 concentration for the Albitite and Fule are identical at 1.93% and vary significantly to the range of the BK25 samples at 4.77-5.79%. MgO concentration indicate depletion in BK25 samples ranging from 0.32-0.35% and indicate comparative abundance in the Fule sample at 1.09% and Albitite sample at 0.92%. K_2O concentration is consistent throughout the hydrothermal samples ranging from 1.19-2.16%. Na_2O concentration vary significantly throughout the hydrothermal samples ranging from 0.38-7.96%, with the BK25-A, BK25-B, BK25-C and Albitite containing similar concentrations of 6.49-7.96% and the Fule depleted at 0.38%. TiO_2 concentration is similar throughout the hydrothermal group ranging from 0.37-1.02%. SiO_2 values vary significantly with the ultramafic Fule at 37.81%, and the remaining hydrothermal samples at an intermediate range of 61.5-66.2%. The BK25-A, BK25-B, BK25-C and Albitite samples indicate similar major geochemistry, in particular the BK25 samples contain minor variability between itself. The Fule indicates the most variable geochemistry of the hydrothermal group.

Copper (ppm) range from 3-1420 in the hydrothermal group, as the Fule and Albitite are depleted in copper ranging from 3-8 and the BK25 sample is enriched ranging between 1100-1420. Nickel (ppm) concentrations are similar throughout the hydrothermal group ranging from 8-13. Lead (ppm) varies significantly from 6-74 in the hydrothermal group and from 21-74 within the BK25 group. Zinc (ppm) display similar concentrations ranging from 10-31. Chromium (ppm) concentration is consistent throughout the hydrothermal group ranging from 80-150. The hydrothermal group transition metal concentration is comparatively similar between samples, with the exception of an elevated copper enrichment in the BK25 samples.

Host Rock Group

The host rock group consist of the proximal Kanmantoo 1, Kanmantoo 2 samples and the distal Kanmantoo 3 and Kanmantoo 4 samples. The Al_2O_3 values ranged from 11.38-16.63% with Kanmantoo 3 and 4 ranging from 11.38-14.91% and Kanmantoo 1 and 2 ranging from 16.31-16.63%. CaO values were similar throughout the host rock samples ranging from 0.26-0.61%. Fe_2O_3 was similar through the host rock samples ranging from 10.38-11.56%. MgO varied between the proximal host rocks at 3.3-3.52% compared to the distal host rocks ranging from 1.56-1.96%. K_2O ranged from 2.48-4.82% in increasing concentration with sample number. Na_2O concentration is depleted throughout the host rock group ranging from 0.03-0.14%. TiO_2 values are consistent throughout the host rock group ranging from 0.59-0.77%. SiO_2 varies from 63.18%-69.48% for distal host rocks and 63.33%-64.15% for proximal host rocks. No distinct correlation exists between the proximal and distal host rock and a consistent variation in SiO_2 abundance. Proximal host rocks are slightly enriched in mafic elements compared to distal host rocks. K_2O and Na_2O concentrations are slightly enriched in the distal samples compared to proximal host rocks.

Transition metal concentrations are present in varying quantities throughout the host rock samples. Copper (ppm) concentrations range from 33-54 throughout host rock samples and no disparity exists between proximal and distal groups. The host rocks display similar nickel (ppm) concentrations varying from 31-47. Lead (ppm) concentrations ranges from <2 to 4 in the proximal samples and are more abundant in the distal samples ranging from 41-67. Proximal and Distal host rocks have similar zinc (ppm) concentration with proximal ranges of 75-109 and distal ranges of 96-110.

Chromium (ppm) concentrations range from 60-100, with Kanmantoo 1, 2 and 4 all containing 100 ppm chromium. With the exclusion of lead concentrations, the host rock group indicates similar quantities of transition metals abundant in proximal and distal samples.

Granite Group

The granite group composed of the Sawpit Granite, Petwood Granite and Thomas Syenite indicate distinct variations amongst themselves. The Al_2O_3 values range from 13.64% for the Sawpit granite to 36.04% for the Thomas Syenite. CaO is significantly higher at 1.24% for the Thomas Syenite than the Sawpit Granite at 0.83% and the Petwood Granite depleted at 0.03%. The Fe_2O_3 value is enriched for the Thomas Syenite at 4.14% and the Sawpit Granite at 3.85% and contrast the Petwood Granite at 1.89%. Furthermore the MgO is enriched in the Thomas Syenite at 1.85% and the Sawpit Granite at 1.68% compared to the Petwood Granite at 0.53%, indicating that the Thomas syenite and Sawpit granite are comparable abundant in mafic minerals and that the Petwood granite is depleted. K_2O is heavily enriched in the Petwood Granite at 13.7% and depleted to similar degrees in the Thomas syenite at 1.33% and the Sawpit granite at 0.35%. Na_2O is depleted in both the Petwood Granite at 0.28% and the Thomas Syenite at 0.97% and enriched in the Sawpit Granite sample at 6.59%. TiO_2 values remained consistent throughout the granite samples ranging from 0.27-0.59%. SiO_2 values range from 71.45% for the felsic Sawpit Granite to 52.01% for the intermediate-mafic Thomas Syenite. The granitic samples indicate variable major elemental geochemistry.

Transition metals concentrations are depleted throughout the granite group samples, specifically the Sawpit Granite and Petwood Granite samples. Copper (ppm) concentrations range from 1-3 for the Sawpit and Petwood granite samples and is 31 for the Thomas Granite. Nickel (ppm) concentrations are similar in the granite group ranging from 18 to 27. Lead (ppm) ranges from 2-4 for the Sawpit and Petwood granite

samples and is more abundant at 20 ppm in the Thomas granite sample. Zinc (ppm) concentrations range from 3-10 for the Sawpit and Petwood granite samples yet is elevated in the Thomas Syenite sample at 60. Chromium (ppm) is the most depleted in the Petwood granite sample at 40 and concentration is consistent in the Sawpit Granite and Thomas Syenite samples ranging between 80-90. The Thomas Syenite stands out as an outlier within the granite group as it is the most enriched in transition metals.

The Delamerian S-type granites indicate Al_2O_3 values ranging from 11.45-19.04%, CaO ranging from 0.37-2.09%, Fe_2O_3 0.36-8.01%, K_2O 3.01-6.95%, MgO 0.19-4.33%, Na_2O 1.25-4.13%, TiO_2 0.04-0.8% and SiO_2 56.11-76.58% (Foden et al., 2002). The Thomas Syenite and Sawpit Granite generally indicate similar values to the ranges observed from the S-type granites, however K_2O values are significantly lower, and Na_2O is moderately depleted in the Thomas Syenite and enriched in the Sawpit Granite in comparison.

5.17. Isotope Results

The $\varepsilon Nd_{t = 500ma}$ values of samples investigated in this study range from -11.4 to -14.9. The hydrothermal group possesses the most juvenile samples indicated by the Fule aluminous vein (-11.4), BK25 mineralized hydrothermal vein (-12.3) and Albitite (-13.4). The granitic group possessed $\varepsilon Nd_{t = 500ma}$ at values positioned between hydrothermal and host rock groups, with the Petwood granite (-12.9), Thomas Granite (-13.1) and Sawpit granite (-14.9). The regional host rocks are on average the least juvenile group with the proximal Kanmantoo 2 indicating $\varepsilon Nd_{t = 500ma}$ (-14.3) and distal Kanmantoo 4 (-14.1). The Fule has an $\varepsilon Nd_{t = 500ma}$ difference of (-2.9) to the proximal host rock and a (-2.7) difference to the distal host rock. The BK25 sample has an $\varepsilon Nd_{t = 500ma}$ difference of (-2.0) to the proximal host rock and (-1.8) to the distal host rock. Sr-Nd isotopes characterise the vein assemblages to indicate the most juvenile source and the host rocks and Sawpit granite to indicate the least juvenile source.

The samples studied in this thesis indicate $^{143}Nd/^{144}Nd$ and $^{87}Sr/^{86}Sr$ isotopic correlation most closely associated with Delamerian S-type granites. Kanmantoo samples studied in the thesis indicate $^{143}Nd/^{144}Nd$ values ranging from 0.5112 to 0.5114 and $^{87}Sr/^{86}Sr$ ratios of 0.695 to 0.732. Delamerian S-type granites exhibit similar $^{143}Nd/^{144}Nd$ values ranging from 0.5112 to 0.5115 and $^{87}Sr/^{86}Sr$ values of 0.717 to 0.724 (see figure 12). I-type granite sources indicate similar $^{87}Sr/^{86}Sr$ concentrations to Kanmantoo mine samples of 0.7046 to 0.7175 but significantly higher concentrations of $^{143}Nd/^{144}Nd$ values ranging from 0.51145 to 0.51185. No trend is present that indicates the Kanmantoo samples studied indicates an I to S type trend and the samples solely constrain themselves to a range of values shared by the Delamerian S-type granites.

6. DISCUSSION

6.1. Summary of Observations from major elements and Minerology

Interpretations

Hydrothermal Group

Sample BK25 is interpreted to be derived from a hydrothermal vein deposited post-regional metamorphism. Hydrothermal fluids interpreted to have intersected zones of structural weakness and precipitated to form chalcopyrite and pyrrhotite. The protolith is the schist that has been intruded by a vein with variable alteration occurring on the vein margins. The BK25 sample is entirely hydrothermal, as is the whole mineralogical assemblage composing quartz, k-feldspar, plagioclase, and muscovite. The hydrothermal input altered the surrounding rock with sericitic and chloritic alteration. Monazite crystal formation occurred at 485.35 ± 2.46 Ma (Kimpton 2018) during post-tectonic Delamerian low pressure-temperature processes. Precipitation of chalcopyrite inferred to of occurred at a similar time.

Sample Fule is interpreted to consist of a protolith comprising a Kanmantoo group metasediment that has been introduced to an aluminium-bearing fluid. The aluminous vein entered the protolith and replaced some of the mineralogy. The corundum is a product of the vein assemblages created by the introduction of an aluminous-rich fluid. The evidence of andalusite indicates the sample was subject to low P-T regional metamorphism and the evidence of corundum indicates the influx of fluid through a hydrothermal vein assemblage. Biotite and muscovite attempt to form a type of foliation, but it is not sufficiently pronounced. The micas are interstitial between coarse grained phases therefore appear to bend around other minerals in the hand sample.

The interpretation of the Sample Albitite (KM2-STH-G) hand sample is that the albite groundmass is indicative of hydrothermalism. The groundmass has an indistinguishable grain size and indicates the sample was subject to hydrothermal alteration in the form of sericite alteration replacing potassium feldspar. The thin section hand sample indicates the evidence of tourmaline, a mineral that is found in granitic pegmatites, hydrothermal grains, metamorphic rocks or metasomatism, or as a result of recrystallization from other grains. Coloured tourmalines occur in the pegmatitic phase (Howie 2005), indicating the final stage of magma crystallization. Evidence of andalusite indicates the rock was formed by a hot fluid intrusion followed or post-dating regional low temperature-pressure metamorphism.

Major element chemistry amongst the hydrothermal group is strongly affected by the minerology of the sample, indicated by the enrichment of copper concentration of 1100-1420 ppm in the BK25 samples (see figure 11) and associated BK25 thin section petrography observing 25% chalcopyrite (see figure 6). The 54.53% Al_2O_3 abundance present in the Fule sample (see figure 9) is highlighted by the 25% corundum minerology observed in the petrography (see figure 6). The major and transitional metal chemistry indicates a homogenous composition present among the BK25A, BK25B and BK25C samples. The BK25A, BK25B, BK25C and Albitite samples indicate Na_2O concentrations of 6.49-7.96% which is confirmed in the thin section with plagioclase composing the bulk minerology of the sample. The results verify the hydrothermal genesis of each sample. Sample BK25 is interpreted to compose solely a hydrothermal sulphide-rich vein assemblage, sample Fule is indicative of an aluminous vein interacting with a protolith that has been regionally metamorphosed and the Albitite

sample indicates a protolith that was subject to hydrothermal alteration in the form of sericite alteration replacing potassium feldspar.

Host-rock Group

Interpretation of the Sample Kanmantoo 1 thin section is that the foliation is more pronounced in the thin section in the KMT-1 sample than the BKDK1 sample due to a different bulk composition. The proximal KMT-1 indicates more defined foliation and significantly larger garnet porphyroblasts in comparison to the distal BKDK1 (see figure 7). Al2O3 and MgO concentration are slightly enriched in Kanmantoo 1 at 16.31% and 3.3% compared to the 14.91% and 1.96% of Kanmantoo 4 and is possibly the reason for the larger garnet porphyroblasts. K_2O is enriched in Kanmantoo 4 in comparison to Kanmantoo 1. Fe_2O_3, CaO, TiO_2 and SiO_2 concentrations are comparable between distal and proximal samples. The proximal BKDK1 sample was subject to regional metamorphism of intermediate to high grade capable of forming staurolite observed within the thin section (see figure 7). The garnet porphyroblasts in distal and proximal samples indicate the regional host rocks were subject to peak intermediate-high P-T conditions. The host rock group is indicated to consist of the Kanmantoo Cambrian Metasediment group that was subject to intermediate P-T conditions as a result of the Delamerian orogeny. Major chemistry and transition metals varies between proximal and distal host rocks in K_2O, MgO and slight Al_2O_3 concentrations, however, have comparable bulk chemical compositions for the most part.

Granite Group

The Sawpit Granite (Daw-Syn) sample interpretation indicates a magmatic-aphanitic texture. The sample appears homogenous in the hand sample. Chlorite is present as a large 1cm grain in the hand sample. The interpretation of this thin section sample is that it has interacted with a hydrothermal fluid. The poorly defined edges of the grains lead to speculation regarding the magmatic formation of the intrusion, posing the question of hydrothermal input. The presence of chlorite can indicate that this sample was subject to hydrothermal alteration or low-grade metamorphic alteration. The Sawpit granite does not present a pristine magmatic mineral assemblage (see figure 8) and provides additional evidence that the sample was subject to a hydrothermal fluid input. Sawpit granite concentrations are enriched in Na_2O at 6.59% and are significantly higher than the Petwood Granite at 0.28% and Thomas Granite at 0.97% (see figure 10). Similarly, the hydrothermal group composing BK25A, BK25B, BK25C and Albitite Na_2O range varies from 6.49-7.96%, a concentration which the Sawpit granite resides within, providing further evidence that the sawpit granite sample is subject to hydrothermalism.

The Thomas Granite sample interpretation indicates that the sample is an igneous rock formed by a magmatic intrusion evident by the sample's phaneritic texture. The composition of the Thomas granite differs to other Kanmantoo group hand samples based on the high proportion of both plagioclase and biotite, opposed to samples consisting of predominantly of quartz-biotite. The homogenous composition indicates the formation by a single magmatic fluid. No evidence of secondary hydrothermal or metamorphic processes present in the specimen. The Thomas granite bulk chemistry resides within known S-type Delamerian granite values (Foden et al., 2002).

The interpretation of the Petwood Granite (KM2-HWY) sample is that the protolith was a magmatic rock enriched in potassium feldspar, crystalized from an igneous intrusion. The country rock was subject an influx of hydrothermal fluids and altered the potassium feldspar to form sericite, evident in (figure 8). The k-feldspar in the sample has been almost completely replaced by sericite but some relict domains still exist. The Petwood granite indicates evidence of tourmaline, indicating a granitic pegmatite, hydrothermal grains, metamorphic rock or metasomatism (Howie 2005). The Petwood granite indicates K_2O concentrations of 13.7% and indicates the source of the sericite-dominated thin section. The Petwood granite is charactered by depletions in the major elements CaO (0.03%), MgO (0.53%), Na_2O (0.28%) that are not as pronounced in the Sawpit Granite (CaO 0.83%, MgO 1.68%, Na_2O 6.59%) and Thomas Granite (CaO 1.24%, MgO 1.85%, Na_2O 0.97%). Furthermore, the Petwood Granite does not coincide with values in the Delamerian S-type granite sample ranges (Foden et al., 2002), providing further evidence that the sample was subject to hydrothermal alteration and that the original mineral assemblage has been completely replaced.

Hydrothermal Sample/Distal/Proximal

The hydrothermal samples analysed within the study were normalized to the proximal and distal host rocks to measure an increase or decrease of trace elements and determine if there is chemical variability due to the influx of a hydrothermal flux (see figure 12). The result indicates an enrichment in La, Ce, Pr, Sr, Nd, Sm and Eu in the Bk25-A,B,C samples, and the Albitite and Fule hydrothermal samples remained consistently depleted in measured trace elements, with the exception of an enrichment of Nb and Sr in the Albitite sample. The mineralizing fluid is therefore theorised to introduce a melt abundant in La, Ce, Pr, Sr, Nd, Sm and Eu when compared to the background host rock present in the Kanmantoo region.

Trace Element Analysis

The Kanmantoo Mine sample trace element chemistry indicates a depletion in trace elements abundance as atomic weight increases (see figure 12) (Hofmann 1988). Strontium represents a negative anomaly, where the previous element Praseodymium indicates concentrations of 20 to 100-fold of the primitive mantle and decreases to a measly 1.3-6.7-fold Sr concentration. The spider diagram returns to a 15 to 60-fold concentration of Neodymium and continues in the general trend of decreasing relative abundance of rare earth element with increasing atomic weight. The A-type and I-type granites both exhibit the same trend of decreasing concentration with atomic weight and with a distinct Sr anomaly, with Sr ranging from a minimum 2.5 to a maximum 28.5 times Sr normalized values in the I-type granites and a minimum of 0.1 to a maximum of 7 in the A-type granite locations. Similarly, the S-type granite data (Foden et al., 2002) indicates a Sr range of a minimum of 1.04 to a maximum of 12.004, correlating

with the negative Sr anomaly range of the Kanmantoo mine samples investigated in the thesis and suggesting a similar degree of mobility (Capo et al. 1998).

6.2. Summary of Isotopes

The εNd age corrected for t=500Ma indicates the most juvenile samples to be the Fule at -11.4, followed by BK25 at -12.3 (See figure 14), indicating the introduction of younger hydrothermal sulphide-bearing and aluminous fluids to the country rocks at the Kanmantoo mine. The following ratios were εNd -12.9 for the Petwood granite, -13.1 for the Thomas Granite, -13.4 for the Albitite, -14.1 for Kanmantoo 4, -14.3 for Kanmantoo 2 and -14.9 for the Sawpit Granite. The Kanmantoo 1 and 4 samples were less juvenile compared the hydrothermal veins at -14.3 and -14.1 respectively, indicating the host rocks existed prior to the introduction of hydrothermal fluids. The interpretation from the Petwood granite indicates the hydrothermal replacement by sericitic alteration and therefore the comparatively juvenile isotope value indicates the fluid interacted after the formation of the host rocks, as does the formation of albite in the Albitite hydrothermal sample. The Sawpit granite however contains a less juvenile concentration than the host rocks yet was interpreted to come into contact with hydrothermal fluid and does not follow the same trend as the rest of the sample set.

The samples studied in this thesis indicate isotopic correlation with Delamerian S-type granites (See figure 14) (Foden et al., 2002). S-type granites are sourced from the partial melting of supracrustal sedimentary rocks that have been through varying stages of weathering (Chappell, B. W., & White, A. J. 2001). S-type granites are enriched in Al_2O_3 and depleted Na_2O, indicated in the Delamerian S-type granite with Al_2O_3 ranges

of 11.45-19.04% and Na_2O concentrations ranging from 1.25-4.13%, with the majority of samples containing approximately 2-3% Na_2O (Foden et al., 2002). The next closest group to the samples studied in the thesis are the I-type Delamerian granites, generated by the melting of igneous rocks (Chappell, B. W., & White, A. J. 2001). The association of the Kanmantoo mine samples with the S-type granites indicates that the source of mineralization was not derived from an I-type igneous source, and therefore was not a consequence of mantle input.

6.3. Kanmantoo Sample and Delamerian Intrusive ages

The Kangaroo Island S-type Granites mark syn-Delamerian orogenic events and provide ages younger than the samples studied in the thesis (Foden et.al., 2002). Delamerian S-type granite Cape Willoughby, earliest of the S-type granites, formed at 509 ± 7 Ma (Foden et al., 2002), Vivonne Bay 503 ± 4 Ma, Stun Sail Boom River suites formed at 504 ± 8 Ma, and Cape Hart 500 ± 7 Ma (Foden et al., 2002). The Kangaroo island S-type granites mark the earliest Delamerian granite formation recorded (Foden et al., 2002) and indicate that the Kanmantoo group sediment as source of the granites, where intra-sample geochemical variations are proposed to be caused by I-type magma mixing or mingling (Foden et.al., 2002).

S-type granite Cape Willoughby is significantly older than the BK25 sample, forming at 509 ± 7 Ma, opposed to the mineralized Kanmantoo sample forming at 485.35 ± 2.46 Ma (see table 1), yet both have similar isotopic compositions (see figure 14). The age data and isotopic data create discrepancies as the isotopic concentration is similar but the formation of the Delamerian supracrustal granites is older. The BK25 sample however correlates both age 485.35 ± 2.46 Ma and isotopic composition (εNd -12.3) at

a more juvenile value than the host rocks KMT1 496.98±2.18 Ma (see table 1) and (εNd -14.9) and BKDK1 499.09±1.54 Ma and (εNd -14.3), of which have similar ages to the younger Kangaroo Island S-type granites (Foden et al., 2002; Kimpton 2018). The Fule sample 498.6 ± 16.7 Ma (see table 1) has the most juvenile isotopic signature of the samples studied (εNd -11.4), however indicates a similar age to the host rocks and Delamerian S-type granites (Foden et al., 2002; Kimpton 2018).

Delamerian I-type granites compose syn-tectonic granites Tanunda 500 Ma, Murray Bridge, (506±1; 495.37±1.14; 495.2±3.7; 492±6; 478±2 Ma), Woodside 500±7 Ma, Monarto 492±6 Ma, and Petrel cove 497.8±2.6 Ma (Foden et al., 1999; Foden et al., 2002; Foden et al., 2006; Foden et al., 2020). The Delamerian I-type granites indicate older ages on average than their S-type counterparts. I-type granites have higher initial εNd values than the S-type granites and elevated Nd Isotopic values, indicating the direct requirement of mantle melts in the production of the Delamerian I-type magmas (Foden et al., 2002).

Post tectonic A-type granites of Mannum, Black Hill (487±5), and other A-type Granite represented in study (485± 2.3)(See appendix)(Foden et al., 2020), are a product of post-convergent extension which enabled mafic melts to elevate themselves in the crust by way of crustal thinning and extensional fracturing (Foden et al., 2002).

The A and I type Delamerian granites are all less juvenile than the Kanmantoo samples regardless of age (See figure 14), whereas S-type granites indicate similar isotopic characteristics and older ages (Foden et al., 1999; Foden et al., 2002; Foden et al., 2006;

Foden et al., 2020; Burtt & Phillips, 2003; Turner & Foden, 1996; Milnes et al., 1977; Alias et al. 2002). The Kanmantoo Cu-Au mine presents a unique challenge correlating a diverse dataset composed of varying ages, with the formation of a deposit characterised by a period subject to a multitude of orogenic events, occurring in a relatively short time period.

6.4. Syngenetic Vs epigenetic Controversy

(Oliver et al., 1998) argues an epigenetic theory for the Kanmantoo Cu-Au deposit, describing the Kanmantoo formation in the Ordovician as characterised by low-pressure regional metamorphism altering pelitic and psammitic rocks, where significant changes occurred in bulk chemistry as a result of fluid infiltration. (Oliver et al., 1998) proposes that the Kanmantoo metasediments underwent three geochemical changes during the Delamerian orogeny, including extensive oxygen isotope variations twenty-kilometres from the region, geochemical and isotopic changes in the form of alteration one kilometre surrounding the orebody, and centimetre to meter-scale changes due to veining within the alteration zone. The model proposes that the mineralization was the result of late to post-peak metamorphic regionally-derived fluid flow infiltration and a local crystalizing magmatic body (Oliver et al., 1998).

(Seccombe et al., 1985) supports a syngenetic model in which pre-existing Cu hosted in existed in country rock prior to the remobilization of disseminated sulphides by a hydrothermal fluid. (Seccombe et al., 1985) concluded that the sulphur was leached from pyritic horizons within the Kanmantoo group during hydrothermal circulation and isotopic variations in the study were accounted for by fluid mixing of a seawater source

(Seccombe et al., 1985; Parker, 1986). The epigenetic model indicates a lack of proximal magmatic intrusion in the formation of the Kanmantoo Cu-Au deposit (Seccombe et al., 1985).

In summary the investigation provided evidence for alteration occurring adjacent 0.5-1.5cm veins observed In the BK25 hand sample and isotopic discrepancies between the BK25 (εNd -12.3) and Fule (εNd -11.4) compared to Kanmantoo 2 εNd (-14.3) and Kanmantoo 4 (-14.1) in the one kilometre scale. The Petwood Granite sample located outside the Kanmantoo tenement indicates k-feldspar that has been almost completely replaced by sericite alteration and the Sawpit Granite located 7km North West contains large chlorite grains, characteristic of hydrothermal alteration and microscopy indicative of the sample not maintaining a pristine magmatic mineral assemblage. Examined Kanmantoo samples indicate $^{143}Nd/^{144}Nd$ isotopic similar to Delamerian S-type granites (Foden et al., 2002) and the proximal host rock KMT1 (496.98±2.18 Ma), distal host rock BKDK1 (499.09±1.54 Ma), Aluminous vein segregation (498.6 ± 16.7 Ma) and the Sawpit Granite (501.0 ± 58 Ma) provide evidence for ages younger than the syn-Delamerian Kangaroo Island S-type granites (Foden et al., 2002), albeit within a close proximity. The BK25 age of (485.35 ± 2.46 Ma) is significantly younger than other samples investigated in the thesis and indicates the mineralization did not occur at the same time as the formation of the host rocks (Kimpton 2018). Evidence of hydrothermalism has been observed in the Sawpit and aluminous vein segregation thin sections (see figure 6; see figure 8) and the syn-tectonic ages infer the ore-bearing fluid was deposited from a syngenetic hydrothermal system (Pollock et al., 2018; Seccombe et al., 1985). The absence of an isotopic signature recognizing an I-type mantle-derived

source amongst the Kanmantoo Cu-Au mine samples indicates the ore-bearing fluid was deposited from a synmetamorphic hydrothermal system (Pollock et al., 2018; Seccombe et al., 1985) and that the source of mineralization was not a consequence of mantle input.

6.5. Summary Paragraph on new findings

- εNd age corrected for t=500Ma indicates the most juvenile samples to be the Fule at -11.4, followed by BK25 at -12.3.
- The samples studied in this thesis indicate isotopic correlation most closely associated with Delamerian S-type granites.
- S-type granite formation occur earlier than the Kanmantoo mine samples at 509 +/- 7 Ma, opposed to the BK25 age of 485.35 ± 2.46.
- The Sawpit granite does not present a pristine magmatic mineral assemblage and provides mineralogical and geochemical similarities to hydrothermal samples.
- The Petwood Granite indicates that k-feldspar in the sample has been almost completely replaced by sericite alteration, but some relict domains still exist**.**
- The source of mineralization was not derived from an I-type igneous source, and therefore was not a consequence of mantle input.
- The absence of an isotopic signature recognizing a nearby mantle-derived source indicates the ore-bearing fluid was deposited from a synmetamorphic hydrothermal system.

7. CONCLUSION

The Kanmantoo Mine Mineralization samples indicates correlation with crustal S-type granite formation processes opposed to an I-type granitic mantle-derived melt or I-S type mantle input. The hydrothermal mineralized sample 'BK25' indicated a more juvenile composition than the host rocks as determined by the εNd value, suggesting the mineralization is a product of the introduction of a younger hot aqueous fluid to an older pre-existing host rock. The data composes a limited sample set but within a small area. The geographically nearest sampled intrusions of 'Monarto', 'Palmer' and 'Rathjen Hill' are of I-type granitic origin and formed from a mantle source. The S-type granites of Kangaroo island are derived from the same Kanmantoo group sediment and indicate similar isotopic compositions, albeit moderately older ages in respect to the Delamerian. The data presents an S-type source within the Kanmantoo vicinity, amidst an Eastern Adelaide Hills region characterised by I-type intrusions. The absence of an isotopic signature recognizing a nearby mantle-derived source indicates the ore-bearing fluid was deposited from a synmetamorphic hydrothermal system.

8. ACKNOWLEDGEMENTS

A sincere thank you to Caitlin Rowett and Peter Rolley and the team at Hillgrove Resources for donating their outstanding resources and knowledge, and my supervisors Dr Lucy McGee and Dr Laura Morrissey for guiding and teaching me throughout my Honours year and adapting in a steadfast professional manner to the changes caused by the 2020 Covid-19 pandemic. The project would not have been possible if it were not for the teaching and guidance of Clean Lab Technician David Bruce, who generously reran sample 'WR3' due to an instrument issue within his own time. I would also like to my sponsor the MinexCRC for funding this project and making this year's research possible and to Derrick Hasterok and Dr Katie Howard for managing the fundamentals of the Honours program, and an extended thank you to Juraj Farkas, Darwinaji Subarkah, Ahmad Abdullah A Redaa, Zara Woolston, Peter Keller and the rest of the geochemical team for assisting the presentation and optimization of my research. Finally, a special thank you to the University of Adelaide for granting me the opportunity to study geology at a tertiary level throughout both my Bachelor's degree and Honours degree.

REFERENCES

Alias, G., Sandiford, M., Hand, M., & Worley, B. (2002). The P–T record of synchronous magmatism, metamorphism and deformation at Petrel Cove, southern Adelaide Fold Belt. *Journal of Metamorphic Geology*, *20*(3), 351-363.

Blewett, R. S., Czarnota, K., & Henson, P. A. (2010). Structural-event framework for the eastern Yilgarn Craton, Western Australia, and its implications for orogenic gold. *Precambrian Research*, *183*(2), 203-229.

Burtt, A. C., & Phillips, D. (2003). Ar/Ar dating of a pegmatite, Kinchina Quarry, Murray Bridge, South Australia. *MESA J*, *28*, 50-52.

Calvo, G., Mudd, G., Valero, A., & Valero, A. (2016). Decreasing ore grades in global metallic mining: A theoretical issue or a global reality?. *Resources*, *5*(4), 36.

Capo, R. C., Stewart, B. W., & Chadwick, O. A. (1998). Strontium isotopes as tracers of ecosystem processes: theory and methods. *Geoderma*, *82*(1-3), 197-225.

Chappell, B. W., & Stephens, W. E. (1988). Origin of infracrustal (I-type) granite magmas. *Earth and Environmental Science Transactions of the Royal Society of Edinburgh*, *79*(2-3), 71-86.

Chappell, B. W., & White, A. J. (2001). Two contrasting granite types: 25 years later. *Australian journal of earth sciences*, *48*(4), 489-499.

Chappell, B. W., & White, A. J. R. (1992). I-and S-type granites in the Lachlan Fold Belt. *Transactions of the Royal Society of Edinburgh: Earth Sciences*, *83*(1-2), 1-26.

Dymoke, P., & Sandiford, M. (1992). Phase relationships in Buchan facies series pelitic assemblages: calculations with application to andalusite-staurolite parageneses in the Mount Lofty Ranges, South Australia. *Contributions to Mineralogy and Petrology*, *110*(1), 121-132.

Foden, J., Elburg, M., Turner, S., Clark, C., Blades, M. L., Cox, G., . . . George, C. J. G. R. (2020). Cambro-Ordovician magmatism in the Delamerian orogeny: Implications for tectonic development of the southern Gondwanan margin.

Foden, J., Elburg, M. A., Dougherty-Page, J., & Burtt, A. J. T. J. o. G. (2006). The timing and duration of the Delamerian Orogeny: correlation with the Ross Orogen and implications for Gondwana assembly. *114*(2), 189-210.

Foden, J., Elburg, M. A., Turner, S., Sandiford, M., O'Callaghan, J., & Mitchell, S. J. J. o. t. G. S. (2002). Granite production in the Delamerian orogen, South Australia. *159*(5), 557-575.

Foden, J., Sandiford, M., Dougherty-Page, J., & Williams, I. (1999). Geochemistry and geochronology of the Rathjen Gneiss: implications for the early tectonic evolution of the Delamerian Orogen. *Australian Journal of Earth Sciences*, *46*(3), 377-389.

Georem.mpch-mainz.gwdg.de. 2020. *Georem - Query By Reference Samples Or Materials (Preferred Values)*. [online] Available at: <http://georem.mpch-mainz.gwdg.de/sample_query_pref.asp> [Accessed 15 September 2020].

Gibson, G. M., & Ireland, T. R. (1996). Extension of Delamerian (Ross) orogen into western New Zealand: Evidence from zircon ages and implications for crustal growth along the Pacific margin of Gondwana. *Geology*, *24*(12), 1087-1090.

Haines, P. W., & Flöttmann, T. J. A. J. o. E. S. (1998). Delamerian Orogeny and potential foreland sedimentation: a review of age and stratigraphic constraints. *45*(4), 559-570.

Hammerli, J., Kemp, A. I. S., & Spandler, C. (2014). Neodymium isotope equilibration during crustal metamorphism revealed by in situ microanalysis of REE-rich accessory minerals. *Earth and Planetary Science Letters*, *392*, 133-142.

Hammerli, J., Spandler, C., & Oliver, N. H. (2016). Element redistribution and mobility during upper crustal metamorphism of metasedimentary rocks: an example from the eastern Mount Lofty Ranges, South Australia. *Contributions to Mineralogy and Petrology*, *171*(4), 36.

Haines, P. W., Flöttmann, T., Gum, J. C., Jago, J. B., & Gatehouse, C. G. (1996). Integrated approach to the reinterpretation of the Cambrian Kanmantoo Group type section, South Australia. In *Geological Society of Australia Abstracts* (Vol. 41, p. 177).

Hofmann, A. W. (1988). Chemical differentiation of the Earth: the relationship between mantle, continental crust, and oceanic crust. *Earth and Planetary Science Letters*, *90*(3), 297-314.

Howie, R. A. (2005). MINERALS| Other Silicates.

Hurlbut, C. S., & Klein, C. (1977). *Manual of mineralogy (after James D. Dana)*. Wiley.

Jago, J. B., Gum, J. C., Burtt, A. C., & Haines, P. W. (2003). Stratigraphy of the Kanmantoo Group: A critical element of the Adelaide Fold Belt and the Palaeo-Pacific plate margin, Eastern Gondwana. *Australian Journal of Earth Sciences*, *50*(3), 343-363.

Jochum, K. P., Weis, U., Schwager, B., Stoll, B., Wilson, S. A., Haug, G. H., ... & Enzweiler, J. (2016). Reference values following ISO guidelines for frequently requested rock reference materials. *Geostandards and Geoanalytical Research*, *40*(3), 333-350.

Kimpton, B. J. (2018). *The geological relationship between Kanmantoo Cu-Au deposit mineralisation, hydrothermal metasomatism and igenous intrusives (Unpublished honours thesis)*. University of Adelaide, Adelaide.

Lovering, T. S. (1963). Epigenetic, diplogenetic, syngenetic, and lithogene deposits. *Economic Geology*, *58*(3), 315-331.

McCulloch, M. T., & Chappell, B. W. (1982). Nd isotopic characteristics of S-and I-type granites. *Earth and Planetary Science Letters*, *58*(1), 51-64.

Milnes, A. R., Compston, W., & Daily, B. (1977). Pre-to syn-tectonic emplacement of early Palaeozoic granites in southeastern South Australia. *Journal of the Geological Society of Australia*, *24*(1-2), 87-106.

Morgan, B. (2019). *Crustal evolution and exploration potential of Delamerian south-eastern South Australia (Unpublished honours thesis)*. University of Adelaide, Adelaide.

Offler, R., & Fleming, P. D. (1968). A synthesis of folding and metamorphism in the Mt Lofty Ranges, South Australia. *Journal of the Geological Society of Australia*, *15*(2), 245-266.

Oliver, N. H. S., Dipple, G. M., Cartwright, I., & Schiller, J. (1998). Fluid flow and metasomatism in the genesis of the amphibolites-facies, pelite-hosted Kanmantoo copper deposit, South Australia. *American Journal of Science*, *298*(3), 181-218.

Parker, A. J. (1986). Tectonic development and metallogeny of the Kanmantoo Trough in South Australia. *Ore Geology Reviews*, *1*(2-4), 203-212.

Pollock, M. V., Spry, P. G., Tott, K. A., Koenig, A., Both, R. A., & Ogierman, J. (2018). The origin of the sediment-hosted Kanmantoo Cu-Au deposit, South Australia: Mineralogical considerations. *Ore Geology Reviews*, *95*, 94-117.

Richards, J. P. (2011). Magmatic to hydrothermal metal fluxes in convergent and collided margins. *Ore Geology Reviews*, *40*(1), 1-26. doi:10.1016/j.oregeorev.2011.05.006

Richards, J. P. (2013). Giant ore deposits formed by optimal alignments and combinations of geological processes. *Nature Geoscience*, *6*(11), 911-916. doi:10.1038/ngeo1920

Robb, L. (2005). Introduction to Ore Formation Processes. In: Blackwell Publishing Company, UK, 373p.

Rogers, A. F., & Tolman, C. F. (1916). Sericite a low temperature hydrothermal mineral. *Economic Geology*, *11*(2), 118-150.

Rötzer, N., & Schmidt, M. (2018). Decreasing metal ore grades—is the fear of resource depletion justified?. *Resources*, *7*(4), 88.

Sandiford, M., Eraser, G., Arnold, J., Foden, J., & Farrow, T. (1995). Some causes and consequences of high-temperature, low-pressure metamorphism in the eastern Mt Lofty Ranges, South Australia. *Australian Journal of Earth Sciences*, *42*(3), 233-240.

Sandiford, M., Foden, J., Zhou, S., & Turner, S. (1992). Granite genesis and the mechanics of convergent orogenic belts with application to the southern Adelaide Fold Belt. *Geological Society of America Special Papers*, *272*, 83-94.

Seccombe, P. K., Spry, P. G., Both, R. A., Jones, M. T., & Schiller, J. C. (1985). Base metal mineralization in the Kanmantoo Group, South Australia; a regional sulfur isotope study. *Economic Geology*, *80*(7), 1824-1841.

Thomson, B. P. (1975). Kanmantoo Trough-regional geology and comments on mineralization. In *Economic Geology of Australia and Papua New Guinea-1. Metals. Australas* (Vol. 5, pp. 455-560).

Tomkins, A. G. (2013). On the source of orogenic gold. *Geology*, *41*(12), 1255-1256. doi:10.1130/focus122013.1

Turner, S., Foden, J. J. M., & Petrology. (1996). Magma mingling in late-Delamerian A-type granites at Mannum, South Australia. *56*(3-4), 147-169.

Turner, S., Kelley, S., VandenBerg, A., Foden, J., Sandiford, M., & Flottmann, T. J. G. (1996). Source of the Lachlan fold belt flysch linked to convective removal of the lithospheric mantle and rapid exhumation of the Delamerian-Ross fold belt. *24*(10), 941-944.

Turner, S. P. (1996). Petrogenesis of the late-Delamerian gabbroic complex at Black Hill, South Australia: implications for convective thinning of the lithospheric mantle. *Mineralogy and Petrology*, *56*(1-2), 51-89.

Witt, W. K., Knight, J. T., & Mikucki, E. J. (1997). A synmetamorphic lateral fluid flow model for gold mineralization in the Archean southern Kalgoorlie and Norseman terranes, Western Australia. *Economic Geology*, *92*(4), 407-437.

Yardley, B. W. D., & Cleverley, J. S. (2015). The role of metamorphic fluids in the formation of ore deposits. *Geological Society, London, Special Publications*, *393*(1), 117-134. doi:10.1144/sp393.5

APPENDIX A: PETROGRAPHY

Appendix Figure A1: Hand Sample Photography of the Kanmantoo Mine Samples. The hand samples entail a sample set of granitic, hydrothermal, and regionally metamorphosed host rocks. Going from Left to Right, Top to Bottom; Kanmantoo 1, Kanmantoo 4, Fule, Thomas Granite, Albitite, Ben Kimpton 25 'BK25', Sawpit Granite. Due to landholder issues the Petwood Granite was unavailable for hand sampling

APPENDIX B: METHODOLOGY

Sample Number Allocated for Thermal Ionization Mass Spectrometer

Table 3: Sample number, rock-type, column number and amount of times placed in the centrifuge prior to commencing column chemistry. Samples that indicated the presence of remaining organics.

had to be placed in the centrifuge twice.

Sample Number	Rock Type	Column Number	Centrifuge Required Once	Centrifuge Required Twice
WR1	Albatite	1		Yes
WR2	BK25	2		Yes
WR3	Fule	3		Yes
WR4	Kanmantoo 2	4		Yes
WR5	Sawpit Granite	5		Yes
WR6	Petwood Granite	6	Yes	
WR7	Thomas Syenite	7		Yes
WR8	Kanmantoo 4	8	Yes	
BHV0-2	Standard -Hawaiian Basalt 1919 (Georem 2020)	9		Yes
Blank-2628	Blank	10	Yes	

Appendix Table B1: Chart of the Kanmantoo mine samples, geological group, and location, indicating which samples were surface grabs All coordinates were taken in Zone 54H Adelaide Hills**.**

Sample	Location	Easting	Northing
Kanmantoo 1	Gps -54h0/6114135 (Utm) Surface Grab	317988	6114135
Kanmantoo 2	GPS – 54h0/317988E/6114135 (UTM) Surface Grab	317988	6114135
Kanmantoo 3	gps – 54H0/6114361 (utm) Surface Grab	318628	6114361
Kanmantoo 4	Gps- 54H0/6114361 (utm) Surface Grab	318628	6114361
Bk25	East Haul Road	318326.8E	6114809N
Fule	-Currently Using BK-BDG1/2 location (South Pit Wall) but double check	318100	6114847
Albitite (Referred to as KM2-STH-G	-As mentioned in Brayden Morgan's Thesis Surface Grab	317469.87	6113094.47
Petwood Granite (Referred to as the KM2-HWY-G)	Surface Grab	313804.34	6115444.03
Sawpit Granite (Referred to as the DAW-SYN)	Surface Grab	315816.16	6120088.00
Thomas Granite		317321	6112723

APPENDIX C: GEOCHEMISTRY

Whole Rock Geochemistry Majors Appendix:

Appendix Table C1

Mine Sample Whole rock Geochemistry

	Al2O3	BaO	CaO	Cr2O3	Fe2O3	K2O	MgO	MnO	Na2O	P2O5	SiO2	SrO	TiO2	LOI	Total
Sawpit Granite	13.64	0.01	0.83	0.01	3.85	0.35	1.68	0.02	6.59	0.14	71.45	<0.01	0.59	0.92	100.15
Fule Al vein	54.53	0.09	0.49	0.02	1.93	2.04	1.09	0.02	0.38	0.35	37.81	<0.01	0.37	1.92	101.1
Petwood Granite	21.32	0.18	0.03	0.01	1.89	13.7	0.53	0.01	0.28	0.02	60.01	<0.01	0.27	1.61	99.98
Albitite	20.97	0.04	0.72	0.02	1.93	2.16	0.92	0.01	7.96	0.11	61.74	0.01	1.02	1.72	99.42
Thomas Syenite	36.04	0.04	1.24	0.02	4.14	1.33	1.85	0.09	0.97	0.45	52.01	0.01	0.37	2.32	100.95
KAN1	16.31	0.03	0.61	0.02	10.38	2.48	3.3	0.24	0.09	0.1	64.15	<0.01	0.74	1.84	
KAN2	16.63	0.04	0.26	0.02	10.76	3.52	3.52	0.21	0.03	0.05	63.33	<0.01	0.77	1.34	
KAN3	11.38	0.06	0.59	0.01	10.48	3.98	1.56	0.11	0.12	0.23	69.48	0.01	0.59	1.98	
KAN4	14.91	0.08	0.3	0.02	11.56	4.82	1.96	0.49	0.14	0.19	63.18	0.01	0.76	1.83	
BK25GC-A	19.05	0.01	0.48	0.011	5.2	1.59	0.32	0.05	7.75	0.19	61.5	0.02	0.65	2.86	99.68
BK25GC-B	16.5	0.01	0.54	0.012	5.79	1.31	0.35	0.07	6.49	0.27	66.2	0.01	0.67	3.15	101.37
BK25GC-C	18.7	0.01	0.51	0.016	4.77	1.19	0.35	0.05	7.71	0.21	64.1	0.02	0.82	2.93	101.39

Appendix table C2

Delamerian A-Type Whole Rock Geochemistry (Foden et al., 2002; Foden et al., 2020):

Pathaway Ridge Type A-type Granites

	Al2O3	BaO	CaO	Cr2O3	Fe2O3	K2O	MgO	MnO	Na2O	P2O5	SiO2	SrO	TiO2	LOI	Total
Cold and Wet	12.32		0.81		1.88	4.84	0.18	0.04	3.49	0.03	74.35		0.16	0.29	98.39
Cold and Wet	13.08		0.85		2.14	5.19	0.22	0.05	3.63	0.03	73.26		0.19	0.29	98.93
Kongal Rocks	11.88		0.13		6.46	3.89	0.06	0.08	0.34	0.01	75.19		0.07	1.51	99.62
Kongal Rocks	12.02		0.22		1.52	4.95	0.04	0.03	3.24	0.01	77.02		0.06	0.5	99.61
Jip Jip	12.7		0.85		1.97	3.04	0.09	0.05	4.72	0.02	74.6		0.14	0.41	98.59
Mt Monster	13.22		0.84		1.97	5.39	0.23	0.04	3.55	0.03	73.71		0.18	0.52	99.68
Mt Monster	13.1		0.85		1.97	5.4	0.2	0.04	3.43	0.03	73.1		0.19	0.66	98.97
Marcollat	12.2		0.64		2.53	5.28	0.08	0.07	3.66	0.02	74.42		0.19	0.14	99.23
Marcollat	12.2		0.62		2.45	5.28	0.05	0.08	3.63	0.02	74.5		0.2	0.23	99.26
Marcollat	12.5		0.59		2.04	5.39	0.04	0.07	3.69	0.02	73.8		0.17	0.27	98.58
Sedan	13.23		1.27		1.57	4.26	0.4	0.04	3.76	0.04	74.41		0.21	0.28	99.47
Monteith	13.89		0.92		1.97	5.25	0.45	0.04	3.9	0.1	71.45		0.37	0.24	98.58

Appendix Table C3

Delamerian I-Type Whole Rock Geochemistry (Foden et al., 2002; Foden et al., 2020):

	Al2O3	BaO	CaO	Cr2O3	Fe2O3	K2O	MgO	MnO	Na2O	P2O5	SiO2	SrO	TiO2	LOI	Total
Pt Elliot	13.2		1.12		0.68	5.63	0.74	0.02	2.62	0.08	73.28		0.33	0.49	99.76
Anabama	17.28		2.93		3.66	3.77	1.51	0.05	3.99	0.16	65.13		0.56	0.8	99.84
Victor Harbor	14		2.68		4.33	4.45	1.59	0.06	2.85	0.15	68.7		0.75		99.56
Reedy Ck	16.2		3.38		4.57	2	1.77	0.06	4.36	0.24	65.6		0.67	1.2	100.05
Tanunda	13.46		2.73		3.94	3.38	1.15	0.04	2.99	0.13	70.49		0.68	0.46	99.45
Tanunda	11.94		0.7		1.69	3.67	0.33	0.01	3.72	0.03	76.75		0.68	0.18	99.31
Tanunda	13.63		1.19		2.52	3.28	0.61	0.01	4.6	0.12	71.59		0.68	1.51	99.75

Appendix Table C4

Delamerian S-Type Whole Rock Geochemistry (Foden et al., 2002; Foden et al., 2020):

	Al2O3	BaO	CaO	Cr2O3	Fe2O3	K2O	MgO	MnO	Na2O	P2O5	SiO2	SrO	TiO2	LOI
VB (Vivonne Bay) (kism-07)	13.59		1.66		3.22	4.04	1.34	0.05	2.77	0.23	71.88		0.51	
SSBR (Stun Sail Boom River) (SS2000-13)	12.27		2.09		4.823	3.01	1.89	0.07	2.26	0.23	71.8		0.76	
Cape Y.H (91-CYH1)	12.8		1.76		3.71	4.01	0.6	0.06	3.36	0.11	72.09		0.46	
CW (Cape Willoughby) (1155-CW2)	13.45		0.37		0.52	4.23	0.22	0	4.13	0.08	75.97		0.09	
SSBR (Stun Sail Boom River) SS2000-16	13.34		1.25		1.743	5.583	0.83	0.03	2.16	0.161	72.86		0.23	
VB (Vivvone Bay) K189-6	13.31		1.84		3.71	3.48	1.67	0.06	2.59	0.07	71.5		0.46	
VB (VB2000-5)	14.32		2.04		5.09	3.495	2.66	0.07	2.12	0.123	67.76		0.64	
VB (VB2000-7)	13.91		1.96		4.084	3.313	1.97	0.07	2.51	0.049	70.96		0.49	
SSBR (SS2000-11)	11.45		1.22		2.403	3.94	1.05	0.04	2.31	0.122	76.28		0.32	
SSBR (MSA-378)	12		1.03		2.18	4.94	0.76	0.03	2.17	0.1	76		0.29	
VB (929-05)	19.04		1.1		8.01	6.95	4.33	0.12	1.25	0.14	56.11		0.8	
VB (Ki–29)	13.61		0.55		0.36	5.13	0.19	0.01	2.81	0.2	76.55		0.04	

Appendix Table C5

Kanmantoo Samples Whole rock Transition Metals Geochemistry:

	SiO2	Cr	Co	Cu	Li	Mo	Ni	Pb	Sc	Zn
Sawpit Granite	71.45	80	66	1	<10	<1	27	2	11	10
Fule Al vein	37.81	100	6	3	70	1	13	6	7	10
Petwood Granite	60.01	40	1	3	10	1	18	4	4	3
Albitite	61.74	150	5	8	10	1	12	6	8	14
Thomas Syenite	52.01	90	9	31	90	2	22	20	8	60
KAN1	64.15	100	15	33	10	1	37	4	12	75
KAN2	63.33	100	16	35	30	1	40	<2	14	109
KAN3	69.48	60	16	30	50	1	31	67	9	96
KAN4	63.18	100	21	54	50	<1	47	41	14	110
BK25GC-A	61.5	80	41	1400	<10	<1	8	74	3	31
BK25GC-B	66.2	90	100	1100	<10	<1	12	21	3	20
BK25GC-C	64.1	110	36	1420	<10	<1	8	29	3	22

Appendix Table C6

Whole Rock Trace Element Reference (Hoffman 1988) Appendix:

	Most incompatible trace elements																		***Least incompatible trace elements***
	Rb	**Ba**	**Th**	**U**	**Nb**	**La**	**Ce**	**Pr**	**Sr**	**Nd**	**Zr**	**Hf**	**Sm**	**Eu**	**Gd**	**Dy**	**Er**	**Yb**	**Lu**
Primitive mantle Hofmann 1988	0.5353	6.049	0.0813	0.0203	0.6175	0.6139	1.6011	0.2419	18.21	1.1892	9.714	0.2676	0.3865	0.1456	0.5128	0.6378	0.4167	0.4144	0.0637

Appendix Table C7

Kanmantoo Sample Trace Elements Appendix:

	SiO2	Rb	Ba	Th	U	Nb	La	Ce	Pr	Sr	Nd	Zr	Hf	Sm	Eu	Gd	Dy
Sawpit Granite	71.45	17.8	40.2	15.35	4.29	12.5	44.4	85.5	11.7	64.3	47	212	5.6	8.67	1.66	7.03	
Fule Al vein	37.81	41.4	732	12.7	1.52	6.1	36.9	74.4	8.71	49.3	33.1	79	2.3	6.77	0.75	5.36	
Petwood Granite	60.01	395	1495	7.71	1.2	6.1	93.9	148.5	13.3	30.4	40.5	64	1.8	4.77	0.65	2.48	
Albitite	61.74	90.1	344	17.85	2.44	18.8	48.8	93.1	10.55	117.5	37.3	241	6.3	6.87	1.32	5.61	
Thomas Syenite	52.01	41.4	351	7.67	1.12	6.6	19.5	43	4.73	83.4	18.2	64	1.8	3.96	0.7	3.71	
KAN1	64.15	133.5	298	14.45	2.72	14.6	37.7	73.7	9.04	49.5	32	211	5.5	6.23	0.93	5.39	
KAN2	63.33	177	349	16.3	2.97	14.9	34.4	66.5	8.24	23.9	29.1	197	5.4	6.1	0.93	4.96	
KAN3	69.48	189.5	511	16.1	4.3	10.9	46.2	88.9	10.9	61.6	38.6	323	8.5	7.68	1.4	6.44	
KAN4	63.18	222	686	19.3	4.55	14.9	54.5	103.5	12.4	78.9	44.3	298	7.9	8.54	1.59	7.4	
BK25GC-A	61.5	72.7	107	18.35	2.4	10.7	86.1	158	15.9	122	59.6	157	4.5	10.45	1.6	7.03	
BK25GC-B	66.2	67.4	87	13.65	2.22	13.7	64.1	118.5	11.95	92	46.2	178	5	8.38	1.35	7.09	
BK25GC-C	64.1	55.7	90	17.65	17.1	16.5	78.6	145	14.8	122	56.4	174	5	9.9	1.52	7.56	

Appendix Table C8

Kanmantoo Mine Samples Normalized to Primitive Mantle Appendix:

	Rb	Ba	Th	U	Nb	La	Ce	Pr	Sr	Nd	Zr	Hf	Sm	Eu	Gd	Dy	Er
Sawpit Granite	33.252382	6.6457266	188.80689	211.33005	20.242915	72.324483	53.400787	48.367094	3.5310269	39.522368	21.824171	20.926756	22.432083	11.401099	13.709048	9.0780809	8.2
Fule Al vein	77.339809	121.01174	156.21156	74.876847	9.8785425	60.107509	46.468053	36.006614	2.7073037	27.833838	8.1325921	8.5949178	17.516171	5.1510989	10.452418	7.4631546	5.7
Petwood Granite	737.90398	247.14829	94.833948	59.1133	9.8785425	152.95651	92.748735	54.981397	1.6694124	34.056509	6.5884291	6.7264574	12.341527	4.4642857	4.8361934	1.7246786	0.9
Albitite	168.31683	56.868904	219.5572	120.19704	30.445344	79.491774	58.147524	43.613063	6.4524986	31.365624	24.809553	23.542601	17.774903	9.0659341	10.939938	8.1843838	7.1
Thomas Syenite	77.339809	58.02612	94.341943	55.172414	10.688259	31.764131	26.856536	19.553535	4.5799012	15.304406	6.5884291	6.7264574	10.245796	4.8076923	7.2347894	5.6287237	4.4
KAN1	249.39286	49.264341	177.73678	133.99015	23.643725	61.410653	46.030854	37.370814	2.7182867	26.908846	21.721227	20.553064	16.119017	6.3873626	10.51092	8.6547507	7.9
KAN2	330.65571	57.695487	200.492	146.30542	24.129555	56.035185	41.533945	34.063663	1.3124657	24.470232	20.280008	20.179372	15.782665	6.3873626	9.6723869	7.7610536	6.9
KAN3	354.0071	84.476773	198.03198	211.82266	17.651822	75.256556	55.524327	45.059942	3.3827567	32.458796	33.250978	31.763827	19.870634	9.6153846	12.558502	9.2975854	7.9
KAN4	414.72072	113.40717	237.39237	224.13793	24.129555	88.776674	64.643058	51.260852	4.3327842	37.251934	30.677373	29.521674	22.095731	10.92033	14.430577	10.990906	8.9
BK25GC-A	135.81169	17.688874	225.70726	118.2266	17.327935	140.25086	98.682156	65.72964	6.6996156	50.117726	16.16224	16.816143	27.037516	10.989011	13.709048	5.3151458	3.0
BK25GC-B	125.9107	14.382543	167.89668	109.35961	22.186235	104.4144	74.011617	49.400579	5.0521691	38.849647	18.324068	18.684604	21.681759	9.271978	13.826053	8.9526497	7
BK25GC-C	104.0538	14.878492	217.09717	842.36453	26.720648	128.03388	90.562738	61.182307	6.6996156	47.426842	17.912292	18.684604	25.614489	10.43956	14.74259	8.1059893	5.6

Appendix Table C9

Delamerian A-type granites Normalized to Primitive Mantle Appendix (Foden et al., 2002; Foden et al., 2020):

	Rb	Ba	Th	U	Nb	La	Ce	Pr	Sr	Nd	Zr	Sm	Eu	Gd	Dy	Er	Yb
Cold and Wet	462.54437	63.481567	492.00492	384.23645	27.692308	94.477928	66.829055	45.473336	1.9769357	36.999664	19.971176	21.992238	6.8681319	19.50078	21.950455	27.597792	28
Cold and Wet	490.56604	69.102331	571.95572	428.57143	29.797571	99.364717	71.82562	43.406366	2.1965953	38.681467	21.721227	20.698577	6.1813187	19.50078	22.734399	28.797696	30
Kongal Rocks	1150.7566	3.6369648	707.25707	684.72906	62.186235	63.528262	58.085067	45.473336	0.1098298	31.954255	11.838583	25.873221	0.6868132	16.575663	18.030731	15.598752	18
Kongal Rocks	823.65029	2.8103819	735.54736	881.7734	56.356275	42.352175	40.59709	33.071517	0.2196595	23.54524	14.618077	20.698577	0.6868132	13.650546	16.462841	16.798656	21
Jip Jip	153.18513	69.432964	190.65191	98.522167	29.959514	73.301841	59.958778	53.741215	3.1850632	43.726875	22.647725	29.754204	12.362637	18.525741	19.59862	20.398368	21
Mt Monster	344.85335	58.191437	360.3936	295.5665	39.838057	130.31438	101.80501	72.343944	2.6908292	48.772284	23.677167	27.166882	6.1813187	15.600624	13.327062	11.519078	11
Mt Monster	280.2167	54.554472	350.55351	231.52709	42.105263	133.57224	224.84542	74.410914	2.7457441	53.817693	22.647725	28.460543	6.8681319	16.575663	14.111007	13.198944	13
Marcollat	200.07472	10.249628	317.34317	270.93596	38.866397	242.71054	170.50778	115.75031	0.4942339	94.180962	42.001235	40.103493	2.7472527	20.475819	12.543117	9.3592513	9.
Marcollat	175.60247	13.225327	301.35301	98.522167	47.773279	244.33947	168.63406	128.15213	0.5491488	96.703666	47.354334	43.984476	3.4340659	21.450858	14.111007	10.799136	10
Marcollat	186.81113	9.9189949	246.00246	108.37438	38.05668	171.03763	124.91412	95.080612	0.6040637	70.635721	40.14824	32.341527	3.4340659	16.575663	10.975227	8.6393089	8.
Sedan	367.08388	75.714994	410.82411	389.16256	46.963563	66.786122	48.091937	28.937578	5.1619989	19.340733	15.750463	12.419146	5.4945055	8.3853354	7.6826591	7.6793856	9.
Monteith	263.96413	106.13325	140.2214	59.1133	70.607287	128.68545	103.67872	64.076064	7.0291049	57.181298	28.103768	31.047865	12.362637	20.475819	18.030731	15.598752	10

Appendix Table C10

Delamerian I-type granites Normalized to Primitive Mantle Appendix (Foden et al., 2002; Foden et al., 2020):

	Rb	Ba	Th	U	Nb	La	Ce	Pr	Sr	Nd	Zr	Sm	Eu	Gd	Dy	Er
Pt Elliot	617.7844	83.98082	392.3739	128.0788	23.96761	65.15719	48.09194	40.51261	3.569467	27.07703	15.23574	16.81759	5.494505	14.04056	10.81844	8.87929
Anabama	290.1177	222.5161	270.6027	275.8621	37.73279	82.91253	59.33421	47.54031	22.18561	30.77699	22.64772	16.30013	9.615385	11.31045	7.996237	6.239501
Victor Harbor	403.1384	121.8383	387.4539	256.1576	28.50202	83.88988	63.08163	53.32782	5.601318	38.59738	32.94215	23.02717	6.868132	18.72075	12.85669	9.599232
Reedy Ck	171.8662	141.6763	36.90037	137.931	21.05263	24.75973	16.86341	12.81521	28.44591	9.754457	14.72102	5.433376	7.554945	4.680187	2.97899	2.159827
Tanunda	227.3492	152.4219	148.8315	108.3744	25.4251	50.49682	42.4708		6.75453	26.06794	29.3391					
Tanunda	269.5685	94.89172	499.385	403.9409	34.97976	78.18863	59.33421		2.47117	28.59065	27.69199					
Tanunda	117.1306	83.48487	279.2128	142.8571	39.83806	61.89933	58.70964		5.985722	36.15876	36.85403					

Appendix Table C11

Delamerian S-type granites Normalized to Primitive Mantle Appendix (Foden et al., 2002; Foden et al., 2020):

S-Type Granite (Cape Younghusband, Cape Willoughby, Vivonne Bay, Stun Sail Boom River)

	Ba	Th	U	Nb	La	Ce	Sr	Nd	Zr	Sm
VB (Kism-07)	87.783105	135.30135	118.2266	24.291498	43.981104	39.347948	8.4568918	21.863438	17.191682	
SSBR (SS2000-13)	85.633989	135.30135	118.2266	24.291498	43.981104	39.347948	8.4568918	21.863438	17.191682	
Cape Y.H. (91-CYHI)	99.024632	397.29397	108.37438	30.283401	125.42759	93.061021	6.0021966	65.043727	34.311303	38.939198
CW (1155-CW2)	99.024632	397.29397	108.37438	30.283401	125.42759	93.061021	6.0021966	65.043727	34.311303	
SSBR (SS2000-16)	189.94875	220.1722	231.52709	12.631579	55.383613	46.218225	10.7743	26.656576	18.107886	16.817594
VB (K189-6)	98.528682			2.1052632	43.981104	41.846231	8.3563976	14.656912	18.015236	9.4178525
VB (VB2000-5)	98.528682	220.1722	231.52709	2.1052632	43.981104	41.846231	8.3563976	14.656912	18.015236	
VB (VB2000-7)	98.528682	220.1722	231.52709	2.1052632	43.981104	41.846231	8.3563976	14.656912	18.015236	
SSBR (SS2000-11)	160.5224	167.28167	93.596059	11.174089	40.723245	34.351383	12.004393	22.704339	17.665225	13.195343
SSBR (MSA-378)	160.5224	167.28167	93.596059	11.174089	40.723245	34.351383	12.004393	22.704339	17.665225	
VB (929-05)	160.5224	167.28167	93.596059	11.174089	40.723245	34.351383	12.004393	22.704339	17.665225	
VB (KI-29)	3.141015	28.290283	88.669951	5.9919028	16.289298	7.4948473	1.0433828	3.6158762	2.1618283	3.4928849

Appendix Table C12

Kanmantoo Hydrothermal Sample Trace Elements Normalized to Host Rock Kanmantoo 4 Appendix:

Samples Normalized by Kan-4

	SiO2	Rb	Ba	Th	U	Nb	La	Ce	Pr	Sr	Nd	Zr	Hf	Sm	Eu	Gd	Dy
Fule Al vein	0.5984489	0.1864865	1.0670554	0.6580311	0.3340659	0.409396	0.6770642	0.7188406	0.7024194	0.6248416	0.7471783	0.2651007	0.2911392	0.79274	0.4716981	0.7243243	0
Albitite	0.977208	0.4058559	0.5014577	0.9248705	0.5362637	1.261745	0.8954128	0.8995169	0.8508065	1.4892269	0.8419865	0.8087248	0.7974684	0.8044496	0.8301887	0.7581081	0.74
BK25GC-A	0.9734093	0.3274775	0.1559767	0.9507772	0.5274725	0.7181208	1.5798165	1.52657	1.2822581	1.5462611	1.3453725	0.5268456	0.5696203	1.2236534	1.0062893	0.95	0.48
BK25GC-B	1.0477999	0.3036036	0.1268222	0.7072539	0.4879121	0.9194631	1.1761468	1.1449275	0.9637097	1.166033	1.0428894	0.5973154	0.6329114	0.9812646	0.8490566	0.9581081	0.81
BK25GC-C	1.0145616	0.2509009	0.1311953	0.9145078	3.7582418	1.1073826	1.4422018	1.4009662	1.1935484	1.5462611	1.2731377	0.5838926	0.6329114	1.1592506	0.9559748	1.0216216	0.73

Appendix Table C13

Kanmantoo Hydrothermal Sample Trace Elements Normalized to Host Rock Kanmantoo 2 Appendix:

Samples Normalized by Kan-2

	SiO2	Rb	Ba	Th	U	Nb	La	Ce	Pr	Sr	Nd	Zr	Hf	Sm	Eu	Gd	Dy
Fule Al vein	0.5970314	0.2338983	2.0974212	0.7791411	0.5117845	0.409396	1.0726744	1.118797	1.0570388	2.0627615	1.137457	0.4010152	0.4259259	1.1098361	0.8064516	1.0806452	0
Albitite	0.9748934	0.5090395	0.9856734	1.095092	0.8215488	1.261745	1.4186047	1.4	1.2803398	4.916318	1.2817869	1.2233503	1.1666667	1.1262295	1.4193548	1.1310484	1
BK25GC-A	0.9711037	0.4107345	0.3065903	1.1257669	0.8080808	0.7181208	2.502907	2.3759398	1.9296117	5.1046025	2.04811	0.7969543	0.8333333	1.7131148	1.7204301	1.4173387	0
BK25GC-B	1.0453182	0.380791	0.2492837	0.8374233	0.7474747	0.9194631	1.8633721	1.7819549	1.4502427	3.8493724	1.5876289	0.9035533	0.9259259	1.3737705	1.4516129	1.4294355	1
BK25GC-C	1.0121585	0.3146893	0.2578797	1.0828221	5.7575758	1.1073826	2.2848837	2.1804511	1.7961165	5.1046025	1.9381443	0.8832487	0.9259259	1.6229508	1.6344086	1.5241935	1

Appendix Table C14

Isotope $^{143}Nd/^{144}Nd$ and $^{87}Sr/^{86}Sr$ Appendix:

	Rb	Sr	Sm	Nd	$^{147}Sm/^{144}Nd$	$^{143}Nd/^{144}Nd$	$^{87}Rb/^{87}Sr$	$^{87}Sr/^{86}Sr$	$^{143}Nd/^{144}Nd_{t=500Ma}$	$^{87}Sr/^{86}Sr_{t=500Ma}$	εNd_0	$\varepsilon Nd_{t=500Ma}$
Albitite	90.1	117.5	6.87	37.3	0.1114380	0.511673	2.236293	0.730178	0.511308	7.14E-01	-18.8	-13.4
BK25	55.7	122	9.9	56.4	0.1062042	0.511710	1.331488	0.732720	0.511363	7.23E-01	-18.1	-12.3
Fule	41.4	49.3	6.77	33.1	0.1237503	0.511816127	2.449037	0.749324	0.511411	7.32E-01	-16.0	-11.4
KAN-2	177	23.9	6.1	29.1	0.1268301	0.511675193	21.782933	0.871786	0.511260	7.14E-01	-18.8	-14.3
Sawpit	17.8	64.3	8.67	47	0.1116109	0.511595967	0.814235	0.719166	0.511230	7.13E-01	-20.3	-14.9
Petwood granite	395	30.4	4.77	40.5	0.0712605	0.511566	38.595377	0.974425	0.511333	6.95E-01	-20.9	-12.9
Thomas	41.4	83.4	3.96	18.2	0.1316465	0.511755	1.474504	0.733103	0.511324	7.22E-01	-17.2	-13.1
KAN-4	222	78.9	8.4	44.3	0.1147258	0.511647	8.205742	0.783697	0.511271	7.24E-01	-19.3	-14.1

Appendix Table C15

Delamerian A-type Samples Isotope Ratios (Foden et al., 2002; Foden et al., 2020):

A-Type Granites (Foden 2020)	$^{143}Nd/^{144}Nd_{t=500Ma}$	$^{87}Sr/^{86}Sr_{t=500Ma}$
Cold and Wet JF07–100	0.511953	0.70631
Cold and Wet JF07–102	0.511952	0.82589
Kongal Rocks JF07-114b	0.511951	0.74979
Kongal Rocks JF07-114a	0.511878	0.7513
Jip Jip JF07–122	0.51205	0.7089
Mt Monster JF07–108	0.511911	0.71378
Mt Monster JF07–109	0.511916	0.70054
Marcollat JF07–116	0.511871	0.68465
Marcollat JF07–117	0.511909	0.63834
Marcollat JF07–119	0.511879	0.71844
Sedan KW08–1	0.511914	0.70424
Monteith KW08–15	0.511917	0.70667

Appendix Table C16

Delamerian I-type Samples Isotope Ratios (Foden et al., 2002; Foden et al., 2020):

I-Type (Foden 2020)		$^{143}Nd/^{144}Nd_{t=500Ma}$	$^{87}Sr/^{86}Sr_{t=500Ma}$
	Pt Elliot A1109–4	0.51174	0.70462
	Anabama A1109/13	0.511596	0.7134
	Victor Harbor BCv35	0.511454	0.71751
	Reedy Ck 779/52	0.511852	0.70605
	Tanunda R14 L1	0.511723	0.71095
	Tanunda R154 L75	0.511829	0.70864
	Tanunda R99 L248	0.511829	0.71526

Appendix Table C17

Delamerian S-type Samples Isotope Ratios (Foden et al., 2002; Foden et al., 2020):

S-type (Foden 2002)		$^{143}Nd/^{144}Nd_{t=500Ma}$	$^{87}Sr/^{86}Sr_{t=500Ma}$
	VB KiSM-34	0.511366	0.72011
	VB KI89-6	0.511286	0.71853
	VB/KI Ki–29	0.511348	0.72359
	Harrow 861-12	0.511545	0.71747
	SSBR SS11	0.511295	0.72026
	SSBR ss11	0.511333	0.7206